International Journal of
Geo-Information

MDPI

Article

Investigating the Spatiotemporal Relationship between the Built Environment and COVID-19 Transmission

Hao Huang [1], Haochen Shi [2], Mirna Zordan [3], Siu Ming Lo [1] and Jin Yeu Tsou [1,*]

1 Department of Architecture and Civil Engineering, City University of Hong Kong, Hong Kong SAR 999077, China; hhuang95-c@my.cityu.edu.hk (H.H.); bcsmli@cityu.edu.hk (S.M.L.)
2 State Key Laboratory of Subtropical Building Science, School of Architecture, South China University of Technology, Guangzhou 510640, China; ar_shc@mail.scut.edu.cn
3 School of Design, Southern University of Science and Technology, Shenzhen 518055, China; mzordan@sustech.edu.cn
* Correspondence: jytsou@cityu.edu.hk

Abstract: Earlier studies have examined various factors that may contribute to the contagion rate of COVID-19, such as urban climatic and socioeconomic characteristics. However, there is a lack of studies at the township level detailing the spatiotemporal settings of built environment attributes, especially in the context of lockdown as a response to the global Omicron outbreak. In this study, we extended the existing literature by relating the initial-stage Omicron pandemic conditions with more comprehensive measures of the built environment, including density, diversity, design, distance to transit, and destination accessibility. The variations from the confirmed clusters of COVID-19 and asymptomatic infected cases before, during, and after the lockdown throughout the Omicron outbreak were identified geographically using GIS methods in 218 township-level divisions across Shanghai during the lockdown period. We also compared the regression results of the ordinary least-squares regression, geographically weighted regression, and geographically and temporally weighted regression. Our results show that (1) among all the built environment variables, metro line length, walking accessibility, hotel and inn density, and population exhibited positive significance in influencing pandemic prevalence; (2) spatial and temporal variations were evident in the association between accessibility, mobility, density-related built environment variables, and COVID-19 transmission across three phases: pre-lockdown, during lockdown, and post-lockdown. This study highlights the importance of targeted public health interventions in densely populated areas with high demand for public transit. It emphasizes the significance of transportation network layout and walking accessibility in controlling the spread of infectious diseases in specific urban contexts. By considering these factors, policymakers and stakeholders can foster urban resilience and effectively mitigate the impact of outbreaks, aligning with the objectives of the 2030 UN Sustainable Development Goals.

Keywords: COVID-19; sustainable development goals; built environment; subdistrict; Shanghai; geographically and temporally weighted regression (GTWR)

check for updates

Citation: Huang, H.; Shi, H.; Zordan, M.; Lo, S.M.; Tsou, J.Y. Investigating the Spatiotemporal Relationship between the Built Environment and COVID-19 Transmission. *ISPRS Int. J. Geo-Inf.* **2023**, *12*, 390. https://doi.org/10.3390/ijgi12100390

Academic Editors: Wolfgang Kainz, Christos Chalkias and Demosthenes Panagiotakos

Received: 24 June 2023
Revised: 18 September 2023
Accepted: 24 September 2023
Published: 27 September 2023

1. Introduction

"Rarely does a resident of any of the world's great metropolitan areas pause to consider the complexity of urban life or the myriad systems that operate round the clock to support it" [1] (p. vii). The COVID-19 pandemic has underscored the importance of investigating the complexity of urban systems, given that urban areas typically serve as the epicenter for the transmission of emerging infectious diseases [2]. This holds true for many metropolitan cities globally, such as New York and London. New York City experienced over one-fifth of the total number of COVID-19 cases and deaths in the United States, which has exceeded 10 million [3]. The city's diverse population includes significant minority communities with notable health and socioeconomic inequalities [4]. Similarly, London stands out within the UK for having the highest proportion of ethnic minority individuals concerning

COVID-19 exposure and mortality risk factors [5]. These cities, usually characterized by their high population density, large-scale population mobility, and hybrid use of land, are more vulnerable in the face of a pandemic. They are more likely to be susceptible to high infection rates and rapid dispraises, creating economic stagnation and posing challenges to the city's public health system [6,7].

The COVID-19 pandemic has disrupted progress toward the United Nations Sustainable Development Goals (SDGs), especially in urban areas with disease transmission epicenters [8,9]. Achieving SDG 3 for good health and well-being and SDG 11 for sustainable and resilient cities and communities will require targeted strategies informed by a nuanced understanding of how built environment factors influence infectious disease spread over time and space. The built environment (BE), which comprises all aspects of our existence, including the artificial surroundings that provide context for human activities, ranging in scale from individual structures and parks or open spaces to whole neighborhoods and cities [10], plays a significant role in shaping a city, it is imperative to explore the relationship between the BE and pandemic prevalence.

Much research has uncovered the hidden transmission mechanisms of COVID-19 inside the BE. Typically, density is a significant urban BE variable that is substantially associated with the proliferation of pandemics [11]. Many researchers have concluded that a greater risk of COVID-19 transmission occurs in more populated and densely populated districts [12–17]. Conversely, Zhang et al. compared the local GWPR and the traditional GLM Poisson regression models to examine the association between sociodemographic factors and COVID-19 incidence. Their results revealed a paradoxical finding where a lower population density in cities was associated with higher COVID-19 incidence [18]. Similarly, Liu's study found a negative relationship between urban areas and population density in relation to the spread of COVID-19 during the early stages of the pandemic [19]. Barak et al. contend that city infection rates are determined by social makeup, politics, compliance, and urban political attributes, challenging the conventional understanding of density as the primary determinant of COVID-19 spread. They argue that population density is conditional in infectious disease transmission [20]. Additionally, other density variables in terms of housing [12,21], healthcare facilities [22,23], commercial facilities [24,25], green space [26,27], and transportation facilities [21,28,29] were found to be related to the spread of COVID-19. Researchers also discovered that indicators such as mixed-use development index, walking accessibility, and the accessibility of healthcare facilities and transit were related to the spread of COVID-19 [29–31]. These studies covered five dimensions: density, diversity, design, destination accessibility, and distance to transit [32–34]. These dimensions are commonly referred to as the 5Ds framework [35–37].

Various methods have been used to investigate the relationship between pandemics and BE. Many scholars have adopted ordinary least-squares (OLS) as their primary study method [11,38]. In contrast, others have used structural equation modeling [24], spatial modeling [39–41], machine learning algorithms [42,43], and geographically weighted regression (GWR) [18,21,22]. As a linear regression technique, OLS does not inherently incorporate spatial relationships or explicitly consider spatial dependencies [44]. While other methods have addressed the spatial relationship between the BE and the spread of COVID-19, they have overlooked the temporal aspect as a significant driver of infection rates. This oversight arises from the fact that COVID-19 cases are distributed spatially and temporally, and the transmission patterns of newly acquired infections may exhibit variability throughout the day and across consecutive days [45]. Chen et al. employed geographical and temporal weighted regression (GTWR) to analyze the impact of population movement on COVID-19 transmission, considering spatial and temporal factors [46]. Their findings indicate that GTWR effectively captures the dynamic and location-specific connections between COVID-19 and population mobility. In a related study, Ling and colleagues developed a mobility-augmented GTWR model to quantify the spatiotemporal influences of social-demographic factors and human activities on COVID-19 dynamics [47].

Further, many studies to date have addressed pandemic transmission at different geographical scales. For example, Sy et al. conducted a macroscale investigation and found that higher-population counties in the United States exhibit higher rates of SARS-CoV-2 transmission through the evaluated data from 3221 counties [48]. In contrast, Credit adopted a community-based microscale approach to examine the relationship between observed COVID-19 testing and case rates in ZIP codes for Chicago and New York [49]. The study's results surprisingly indicated that the ZIP codes with the highest case rates tend to have lower population densities, pedestrian and bike commuting rates, and median incomes. Previous studies on urban density focused on larger areas, but examining specific temporal and locational data is necessary to understand density variations within cities. Aggregated densities at the city or county level are inadequate for assessing health risks related to person-to-person interactions. Population density varies within counties, and models should consider finer spatial resolutions, such as the sub-county level, for accurate COVID-19 analysis [50,51]. China's 'grid governance' scheme, integrating community support and control functions at the district, street, and residential community levels, has effectively managed the COVID-19 outbreak since its inception [52]. Accordingly, investigating mesoscale areas such as administrative districts at or below the county level (e.g., township-level divisions) is optimal for separating urban density's impact relative to internal and external connections.

The global COVID-19 pandemic led to various prevention and control measures implemented in different regions. Heterogeneity in COVID-19 transmission patterns was influenced by urban complexity and population mobility. Earlier studies have examined various factors that may contribute to the contagion rate of COVID-19, such as urban climatic and socioeconomic characteristics. However, research on the spatiotemporal influence of BE factors on COVID-19 transmission is still limited, especially using multi-source big data analytics approaches. Table S1 presents a comprehensive summary of scholars' research on COVID-19, including the geographical scope, research methods, variables, and notable findings. This compilation is based on an extensive review of the relevant literature.

This research aims to fill the gaps in the existing literature by utilizing GTWR to investigate the spatiotemporal relationships between BE attributes and COVID-19 spread to provide data-driven insights for enhancing pandemic preparedness and response. Specifically, our study incorporates time latency as a contributing factor and a location parameter to account for spatial heterogeneity before, during, and after the Shanghai lockdown during the Omicron outbreak. The findings highlight the significance of geographic and temporal context in shaping transmission dynamics. The GTWR model, at the township level, can effectively account for both temporal and spatial heterogeneity and accurately identify the uneven distribution of COVID-19 cases and the complex relationship between its risk factors. The results emphasize the need for tailored interventions based on place-specific relationships and temporal shifts rather than one-size-fits-all measures. Overall, the study generates evidence to guide resilient urban planning and policymaking aligned with SDG 11. The data-driven understanding of how BE factors influence infectious disease transmission can inform targeted improvements to urban form, mobility networks, and access to services to mitigate pandemic impacts.

The remainder of this paper is structured as follows. In Section 2, the study area and dataset are introduced, as well as the research framework and regression analysis. Section 3 describes the basic framework of the GTWR model and its counterpart models used in the study, such as OLS and GWR. The results of the three regression models are also compared and assessed. In Section 4, the key findings from the coefficients of the GTWR model are analyzed in detail, both temporally and spatially. The conclusions and suggestions for future research are summarized in the last part of the paper.

2. Methodology

As a leading global city, Shanghai has pursued rapid urbanization and economic growth, resulting in high population density and an extensive transportation infrastructure. However, these attributes may contribute to infectious disease transmission. This study uses diverse data sources and analytical techniques to investigate spatiotemporal correlations between factors in the BE and COVID-19 transmission at the township level across Shanghai. The collected data includes COVID-19 case counts, demographic and economic variables, and a comprehensive set of BE metrics encompassing density, diversity, design, destination accessibility, and distance to transit measures. Understanding the associations between urban form metrics and pandemic spread can inform targeted interventions aligned with Shanghai's objectives for sustainable development.

The methodological framework, presented in Figure 1, outlines the key processes of compiling data from various sources, including BE, socioeconomic, and COVID-19 case data (Table S2). Data cleaning and variable selection procedures were implemented to address issues such as multicollinearity and enhance model parsimony. Spatial autocorrelation analysis facilitated the exploration of spatial relationships among variables. The regression techniques allowed for comparative modeling of the spatially and temporally varying connections between the urban environment and COVID-19 transmission.

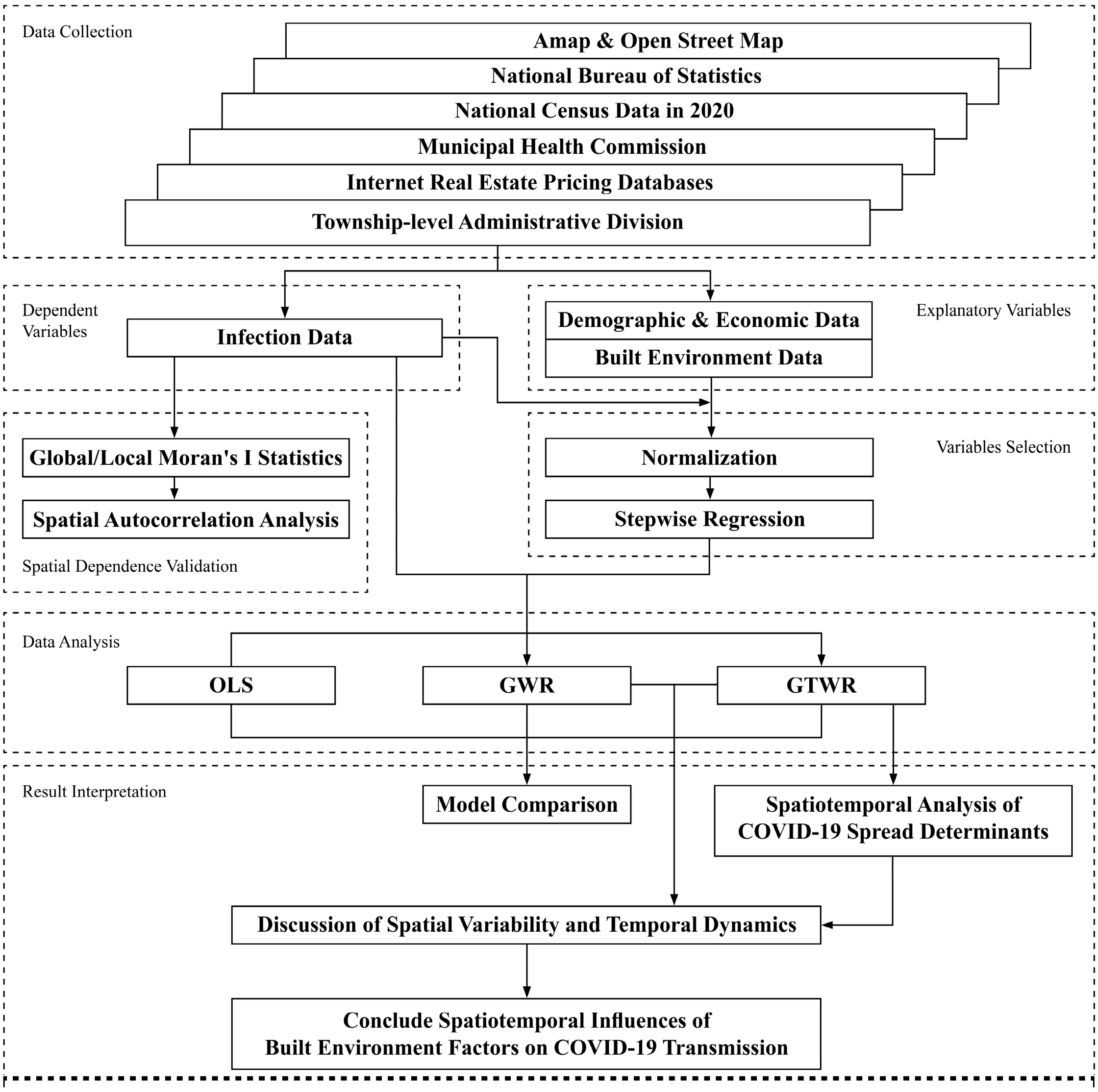

Figure 1. The framework of the research design.

2.1. Study Area

Shanghai is a megacity with over 25 million residents and a land area of 6341 km^2, which is divided into 16 districts (substantially bigger than US counties) and 218 township-level divisions (including subdistricts or towns). The main ring roads within the inner city of Shanghai spread out from the inner ring road in the order of the middle ring road, the outer ring road, and the suburb ring expressway (Figure 2).

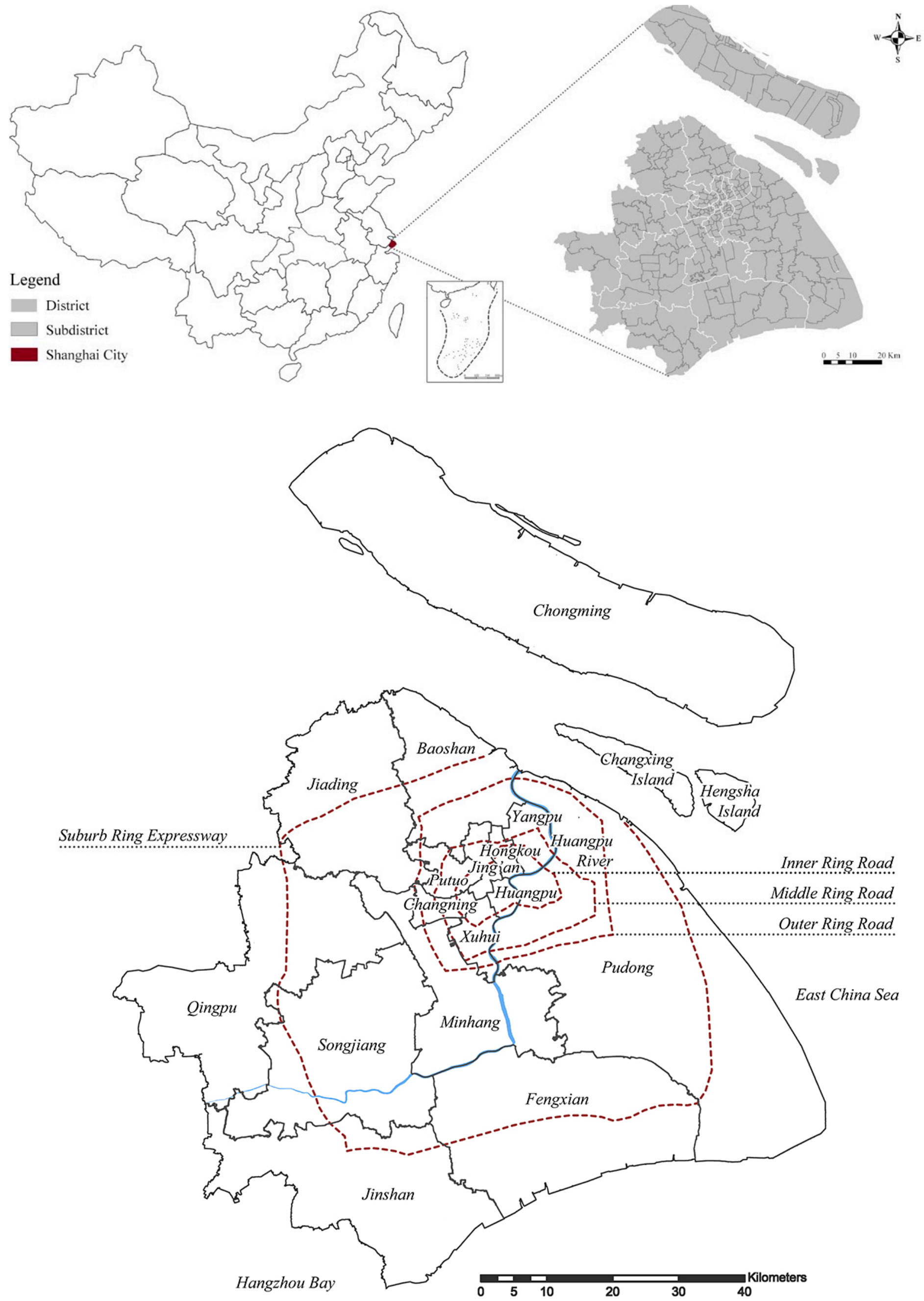

Figure 2. 218 township-level divisions of 16 districts in Shanghai.

In February 2022, Shanghai experienced a new outbreak of COVID-19 caused by the Omicron variant of the SARS-CoV-2 virus. The government responded by locking down different parts of the city at different times, with the entire city being locked down from 1 April 2022. The lockdown was lifted after 95 days. Until 31 July 2022, Shanghai had 650,464 positive cases, peaking at 5487 daily on 28 April 2022. Most locations had three levels of management: closed, control, and prevention. Asymptomatic infections peaked at 25,173 per day on 13 April 2022, then slowly dropped (Figure 3). The government began loosening restrictions in May 2022, and the city gradually restored regular production and living order after 1 June.

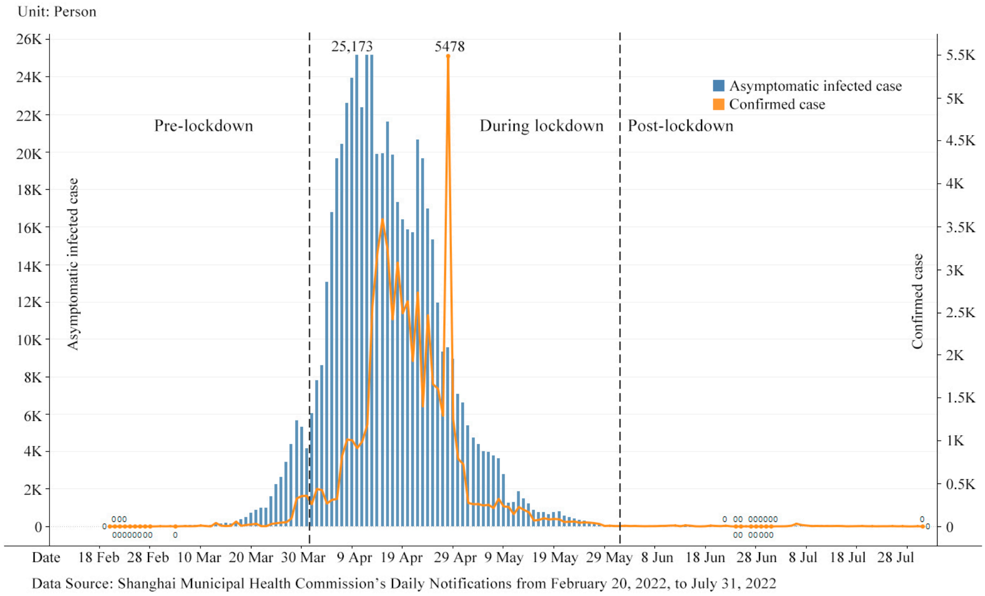

Figure 3. Shanghai COVID-19 case statistics.

2.2. Datasets

2.2.1. Infection Data

Using our proposed method, we analyzed daily infection counts disclosed by the Shanghai government and measured phase shifts in the COVID-19 pandemic timeline. We obtained COVID-19 case data from the Shanghai Municipal Health Commission's daily notifications between 20 February 2022 and 31 July 2022 in 16 districts and used ArcMap 10.8 to geocode each infected community's address to a spatial location with latitude and longitude for visualization. To ensure accurate comparisons of monthly results between March and July, we linked the number of infected individuals in each subdistrict or municipality to the polygon attribute matrix. This allowed us to determine the number of monthly and cumulative infections for each division.

2.2.2. Demographic and Economic Variables

We estimated the population of township-level divisions in 218 selected census tracts within Shanghai's administrative divisions using the preliminary results of the 2020 Chinese Census. Internet real-estate pricing databases, such as Anjuke and Lianjia, were utilized to calculate the average rental and lodging costs. After data cleaning, individual residential unit rents and prices were mapped to their corresponding subdistricts or towns, and average values were calculated.

2.2.3. Built Environment Variables

We quantified the BE variables using the 5Ds framework and summarized the BE indicators, descriptive statistics, and calculation processes in Table 1. During the preparation stage, GIS was instrumental in rapidly collecting and screening urban setting and spatial attribute data from multiple sources. To measure the BE variables, we utilized points of interest (POIs) data, a type of urban big data that accurately depicts the spatial distribution of entities and functional facilities that support human activities in urban environments [53–56]. We obtained the POIs dataset 2022 from Amap, one of China's most popular online map services [57,58]. We calculated the building area, urban greenery, water body area, and transportation network density using vector polygons extracted from the Open Street Map database.

Table 1. BE variables based on 5Ds dimension.

Classification	Variable	Calculation Process
Density	Population density	Total population divided by area.
	Building density	Building square footage divided by area.
	Green space density	$D(GS_j) = \frac{\sum_{k=1}^{n} x_k}{A_j}$ (1) where X_k (k = 1, 2, ..., n) denotes the area of a single green space, n indicates the number of green spaces within the same subdistrict/town, and A_j measures the area of subdistrict/town j.
	Density of road length	$D(Rd_j) = \frac{\sum_{k=1}^{n} x_k}{A_j}$ (2) where X_k (k = 1, 2, ..., n) denotes the length of a single road segment after being divided by administrative boundaries of subdistrict/town j, n indicates the number of roads within the same subdistrict/town, and A_j measures the area of subdistrict/town j.
	Density of bus line length	$D(BusLine_j) = \frac{\sum_{k=1}^{n} x_k}{A_j}$ (3) where X_k (k = 1, 2, ..., n) denotes the length of a single bus line segment after being divided by administrative boundaries of subdistrict/town j, n indicates the number of bus lines within the same subdistrict/town, and A_j measures the area of subdistrict/town j.
	Density of metro line length	$D(MetroLine_j) = \frac{\sum_{k=1}^{n} x_k}{A_j}$ (4) where X_k (k = 1, 2, ..., n) denotes the length of a single metro line segment after being divided by administrative boundaries of subdistrict/town j, n indicates the number of metro lines within the same subdistrict/town, and A_j measures the area of subdistrict/town j.
	Density of bus stop/metro station/road intersection	$D(BusS_j/MetroS_j/RdInter_j) = \frac{N_j}{A_j}$ (5) where N indicates the number of bus stops/metro stations/road intersections within the subdistrict/town j, and A_j measures the area (unit: km^2) of subdistrict/town j. The unit used is number/km^2.
	Density of 12 categories * of POI datasets	$D(POI_{k,\ j}) = \frac{N_k}{A_j}$ (6) where N indicates the number of category k points within the subdistrict/town j, and A_j measures the area (unit: km^2) of subdistrict/town j. The unit used number/km^2.
Design	Quantity of road length/bus line/metro line/bust stop/metro station/road intersection	The quantity of road length/bus line length/metro line length was measured as the total length of road/bus line/metro line within each subdistrict or town, while the quantity of bus stop/metro station/street intersection was the number of street intersections in each subdistrict.
	Green space area, waterbody area	The total area of polygons with green space and waterbody attributes was calculated within the subdistrict/town area.
	Quantity of 12 categories * of POI datasets	The amount of 12 categories of POIs within each subdistrict was counted separately.

Table 1. *Cont.*

Classification	Variable	Calculation Process
Destination accessibility	Accessibility to hospital/clinic, accessibility to kindergarten/school, commuting accessibility, accessibility to park	Opportunity-based measures could simply be to find the nearest destinations to an origin and calculate their distances or to count the number of destinations or opportunities available within a specified distance from an origin [59–62].
		$A_i = \begin{cases} \sum_j M_j, & if\ d_{ij} \leq L \\ 0, & if\ d_{ij} > L \end{cases}$ (7)
	Walk accessibility, drive accessibility, radius setting: 500 meters and 10 kilometers	Betweenness was utilized to describe the road network accessibility [63]. It computes the number of times each street x is traversed by the shortest path between any two street segments, y and z, within a defined analysis radius.
		$\text{Betweenness}(x) = \sum_{y \in N} \sum_{z \in R_y} W(y)W(z)P(z)OD(y,z,x)$ (8)
		where $\text{OD}(y,z,x) = \begin{cases} 1, & \text{if } x \text{ is on the first geodesic found from } y \text{ to } z \\ 1/2, & \text{if } x = y \neq z \\ 1/2, & \text{if } x = z \neq y \\ 1/3, & \text{if } x = y = z \\ 0, & \text{otherwise} \end{cases}$ (9)
Distance to transit	Distance to bus stop/metro station	$DOT(x) = \sum_{y \in Rx1} \frac{p(y)}{d(x,\ y)}$ (10)
		p(y) represents the weight of node y within a radius of R in the equation, where *p(y)* takes on values between 0 and 1. *d (x, y)* is the minimum topological distance between nodes x and y. In our study, *p(x)* indicates the community, *p(y)* depicts the metro station or bus stop, and *R* is 1 kilometer or 15 minutes of walking.
Diversity of land use	Land use mix	The Shannon Entropy Index was used to quantify the land use mix [64]:
		$DI_k = -\frac{\left(\sum_{i=1}^{M} P_{k,i}\ In\ P_{k,i}\right)}{In\ M}$ (11)
		where $P_{k,\ i}$ is the quantity of POIs within subdistrict *k*, which belongs to sub-category *i* as a percentage of the total amount of POIs in subdistrict *k* and denotes the number of POI sub-categories in subdistrict *k*.

Notes *: 12 categories of POI datasets, which are tourist attractions and scenic spots, shopping venues, science, education, and cultural buildings, hotels and inns, public toilets, companies and enterprises, administrative authorities and social groups, residential quarters, restaurants, cafes, and bars, living service facilities, healthcare facilities, and sports and leisure facilities, where *k* is one of the categories.

2.3. Methods

All variables were logarithmically transformed and normalized before further modeling. We employed min-max normalization to mitigate the undesirable effects of sample data. Undesirable effects of sample data encompass outliers and unequal feature scales. Outliers deviate significantly from the majority and can distort the analysis. Min-max normalization addresses outliers by compressing data within a specific range. It also standardizes feature scales for comparability [65–67]. Stepwise regression was utilized to select superior predictors from a larger set of potential predictors to avoid overfitting the data and prevent misleading variable importance regression [68–72]. A total of 54 initial explanatory variables were screened, resulting in the exclusion of 45 and the final selection of the nine most relevant variables (Figure 4). To ensure the absence of multicollinearity, we conducted a variance inflation factor (VIF) test, removing variables with VIF values greater than five from the models [73–75].

We employed OLS regression to examine the relationship between BE and the spatiotemporal distribution of infection populations in 218 township-level divisions (as shown in the following formula) using nine independent variables. The global model assumed that the relationship between the response and explanatory variables did not vary spatially across the study area. To account for spatial nonstationarity, we utilized GWR, which associates explanatory variables with geographic locations but cannot handle temporal nonstationarity [47,76]. This can be viewed as an extension of OLS models by associating explanatory variables with geographical locations, which takes the following form [66,71,72]:

$$Y_i = \beta_0(u_i, v_i) + \sum_{k=1}^{k} \beta_k(u_i, v_i) X_{ik} + \varepsilon_i \tag{12}$$

where i (i = 1, 2, ..., n) denotes a subdistrict or a town, Y_i is the dependent variable (the infected population), (u_i, v_i) denotes the coordinates of point i in space, $\beta_0(u_i, v_i)$ represents the intercept value (constant), and $\beta_k(u_i, v_i)$ is the local regression coefficient of *k-th* explanatory variable in the location (u_i, v_i). X_{ik} is the value of the *k-th* explanatory variable, and ε_i is the error term. Unlike the 'fixed' coefficient estimates over space in the global model, this model allows the parameter estimates to vary across space and is, therefore, likely to capture local effects [72,77].

To explore the relationship between the infected population and its influential variables while considering both spatial and temporal heterogeneity [46,78,79], we adopted the GTWR model proposed by Huang et al. [77]. A typical GTWR model can be written as follows:

$$Y_i = \beta_0(u_i,\ v_i,\ t_i) + \sum_{k=1}^{k} \beta_k(u_i,\ v_i\ t_i)\ X_{ik} + \varepsilon_i \tag{13}$$

For each observation i (i = 1, 2, ..., n), Y_i is the dependent variable, whereas X_{ik} is the k *-th* explanatory variable. (u_i, v_i, t_i) represents the space-time coordinates of observation i; u_i and v_i are the projected spatial coordinates, whereas t_i is the projected temporal coordinate. $\beta_0(u_i, v_i, t_i)$ is the intercept value, and $\beta_k(u_i, v_i, t_i)$ denotes the regression coefficient, which is a parameter measuring the influence of explanatory variable X_{ik} on dependent variable Y_i, and ε_i denotes the error term for observation i [46,80,81].

The GWR-based technique enables visual analysis by generating local parameter estimates that can be displayed on maps [78]. In the case of the GTWR model, each township-level division is associated with a set of coefficients for different variables, including coefficients for each time step. These coefficients can be categorized into intervals and represented using various colors, allowing for visualizing spatial variations in the impacts of BE variables on infections. Additionally, the GWR-based spatial autoregressive modeling incorporates both conditional and unconditional local spatial autocorrelation measures [82], which unveil hidden local patterns in the distribution of variables.

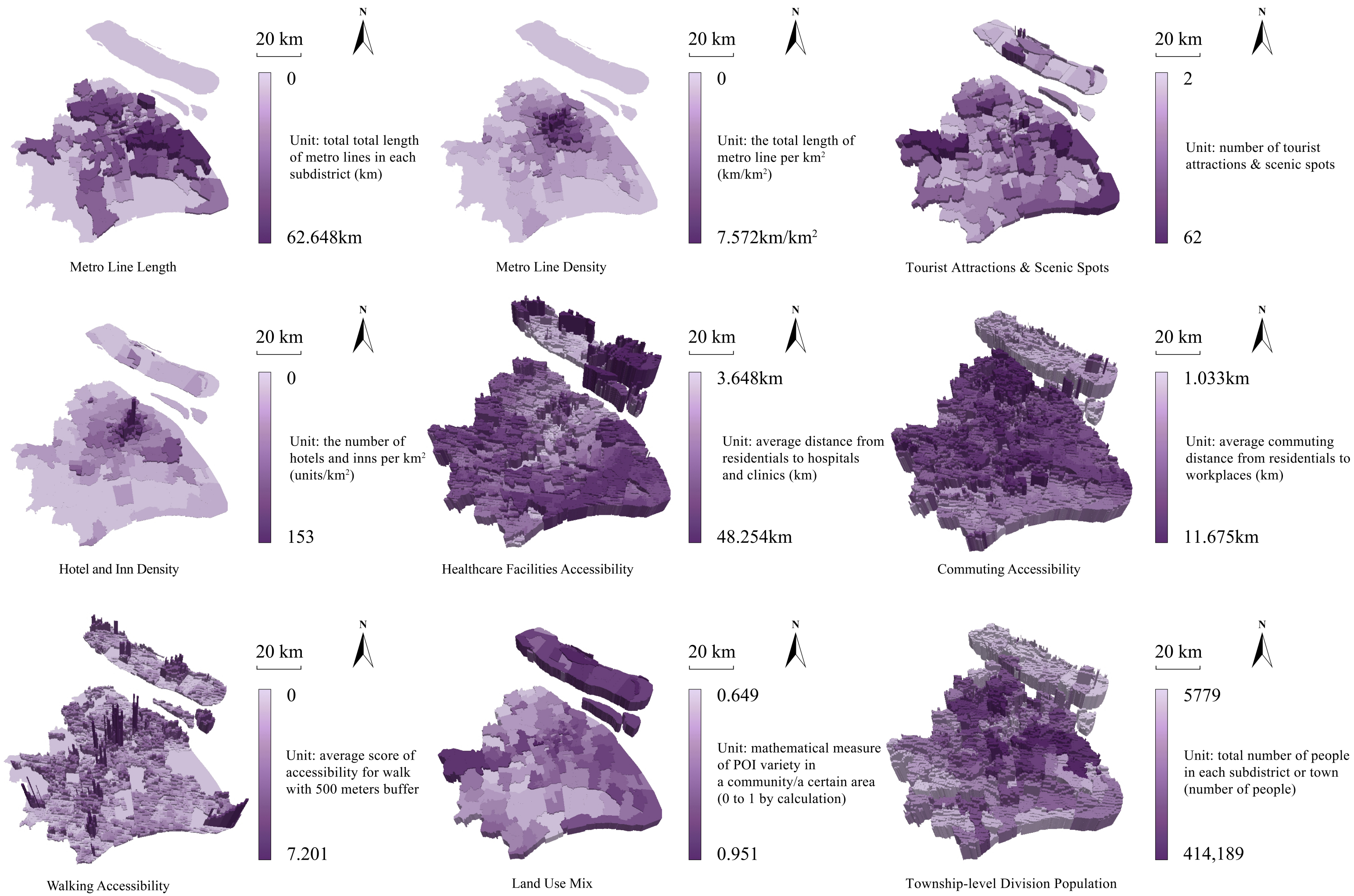

Figure 4. Spatial distribution of selected variables.

Spatial autocorrelation refers to the extent to which a specific sub-region is similar to or different from its neighboring sub-regions regarding a given indicator. This autocorrelation can be assessed on a global and local scale. Global measures provide an overall summary of spatial autocorrelation, while local measures evaluate autocorrelation within specific areas of interest [83,84].

In this study, we computed Moran's I, along with Moran scatter plots and the local indicator of spatial association (LISA). The Moran Index offers a comprehensive assessment of spatial autocorrelation [85], while Moran scatter plots visually represent spatial relationships and facilitate the examination of potential local clusters [86]. By utilizing LISA, we can consider the localized impacts of the phenomenon [87,88]. The LISA clusters are categorized as high–high (HH), low–low (LL), low–high (LH), and high–low (HL). HH and LL clusters indicate significant spatial clusters surrounded by neighboring clusters with either high or low values, respectively [14].

3. Results

3.1. Spatial Patterns: Cluster Analysis

In our exploratory spatial data analysis, we examined the spatial distribution of infected populations at the township-level division. We aimed to identify patterns of aggregation or anomalies. To assess spatial autocorrelation, we generated an empirical distribution by simulating 999 random maps using the infected case numbers and calculating Moran's I for each map. The left panel displays the grey empirical distribution, while the blue line represents the mean. In contrast, the red line represents Moran's I calculated for the variable based on the observed dataset's geography. Figure 5a indicates significant autocorrelation (Moran's I = 0.48, $p < 0.001$), highlighting the high spatial correlation of COVID-19 cases between township-level divisions. The observed pattern's value is significantly higher than that under randomness. This insight is further confirmed in the right panel, which presents a Moran scatter plot illustrating the relationship between the attribute values at each location and the average value of the same attribute in neighboring locations. Figure 5b depicts the scatter plot, with the horizontal axis representing the observation values (response axis) and the vertical Y axis representing the weighted average or spatial lag of the corresponding observation. Positive spatial autocorrelation is observed in the upper-right quadrant, where the attribute's value and local average value are higher than the overall average. Similarly, the lower-left quadrant indicates negative spatial autocorrelation. These findings support the presence of spatial autocorrelation [88,89].

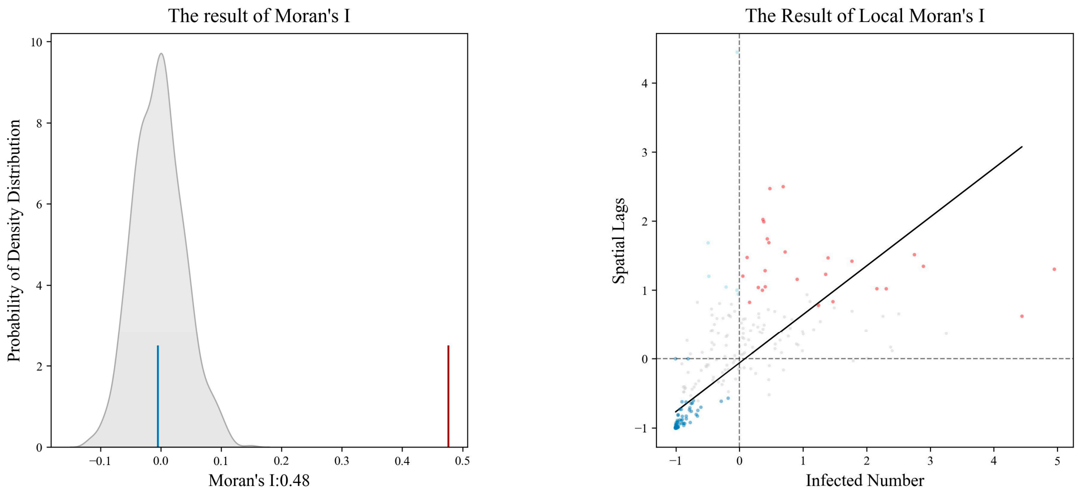

(**a**) (**b**)

Figure 5. (**a**) Moran's I statistics; (**b**) Moran scatter plot.

To analyze the significance of spatial clusters, we employed the LISA in addition to the Moran scatter plot. The LISA cluster map visually represents hot spots, indicating areas with significant clustering. The LISA cluster map of the number of infected cases reveals hot spots in the downtown area of Pudong New Area and along the Huangpu River. In these regions, the HH category (red) represents areas with a high number of confirmed cases, exceeding the average, surrounded by neighboring regions with similarly high numbers. Conversely, the LL category (blue) denotes regions with a low number of confirmed cases, below the average, surrounded by neighboring regions with similarly low values. The LL category is primarily observed in the outskirts of Shanghai, with a few instances of the LH category distributed along the Huangpu River (Figure 6). These findings shed light on the spatial distribution and clustering patterns of infected populations in Shanghai, providing valuable insights for targeted interventions to control and prevent the spread of infectious diseases.

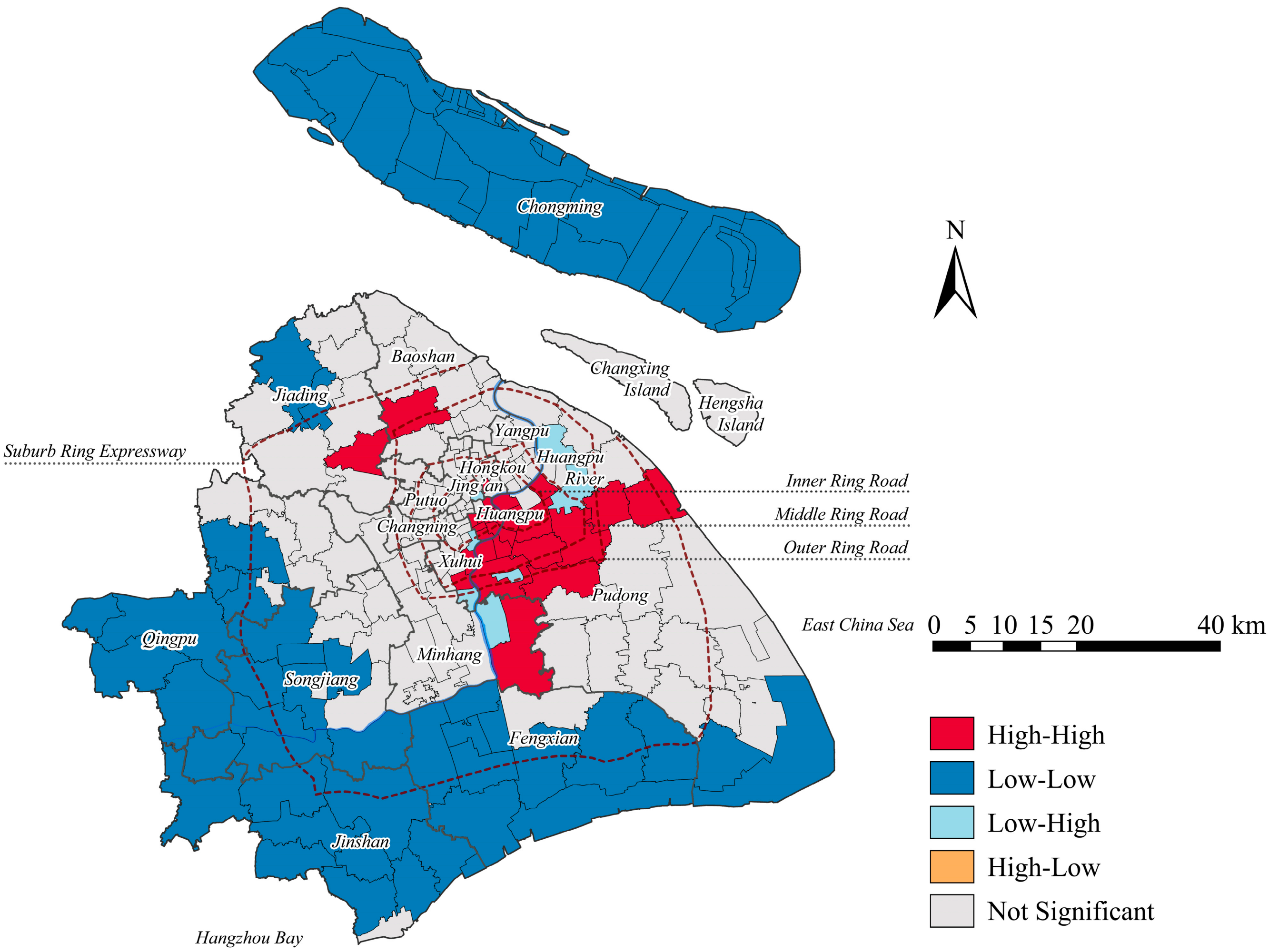

Figure 6. LISA clustering of infected populations in 218 township-level divisions.

3.2. Regression Results and Comparison

To evaluate a model, it is necessary to conduct a test for the serial correlation of residuals [90]. Spatial autocorrelation analysis is commonly used to test the serial correlation of residuals in spatial analysis [91]. Moran's index, a generalization of Pearson's correlation coefficient, is often employed to evaluate spatial clustering effects not captured by the model. A value close to 1 indicates cluster patterns in the residuals, suggesting model inaccuracies and the influence of unaccounted spatial variables. Conversely, a value close to -1 suggests discrete patterns, indicating missing variables contributing to observed spatial patterns. A value close to or equal to 0 indicates a random pattern, implying a better model fit [92,93].

Spatial effects, encompassing spatial autocorrelation and heterogeneity, are integral in modeling. Neglecting these effects during the modeling process leads to misleading significance tests and suboptimal model predictions [94]. In our study, the residuals from three models (OLS, GWR, and GTWR) demonstrated an improvement in model effectiveness, as evidenced by the transition from strong spatial autocorrelation to a random pattern (Table 2). Due to the low adjusted R^2 value observed in the OLS model, the inclusion of an appropriate spatial model is necessary. Although the GWR model demonstrated relatively higher R^2 values for spatial variables, the residuals exhibited dispersed spatial autocorrelation, suggesting the existence of unaccounted variables [14,95]. In contrast, the GTWR model, which incorporates temporal effects in addition to spatial nonstationarity, resulted in a better fit and demonstrated a random pattern in the residuals.

Table 2. Spatial autocorrelation results of OLS, GWR, and GTWR models.

	OLS	**GWR**	**GTWR**
Moran's Index:	0.050	−0.022	−0.001
Expected Index:	−0.005	−0.005	−0.001
Variance:	0.000	0.000	0.000
z-score:	4.112	−1.924	0.160
p-value:	0.000	0.054	0.873
Pattern:	Clustered	Dispersed	Random

The global OLS regression model acts as a reference by which to evaluate the efficacy of local modeling techniques, revealing connections between COVID-19 outbreaks and other BE variables. Table 3 presents the estimated results of the OLS model, indicating an adjusted R^2 value of 0.688, which explains 68.8% of the overall variability in the cumulative case counts. The VIF values of independent variables were all less than 5, indicating no significant multicollinearity among independent variables. Walk accessibility, population, length of metro lines, and density of hotels and inns were strongly positively correlated with COVID-19 cases (p-value < 0.001), while density of metro lines, number of scenic spots, density of shopping services, and accessibility to healthcare services showed a negative correlation with COVID-19 infection. Additionally, work commuting accessibility and the mixability of land use positively influenced the spread of COVID-19 based on coefficient and t-probability.

Table 3. Selected variables and results of stepwise OLS regression.

	Unstandardized Coefficients		**Standardized Coefficients**				
Variable	**B**	**SE**	**Beta**	**t**	**Sig.**	**Tolerance**	**VIF**
(Constant)	−0.139	0.053		−2.630	0.009 **		
Walking accessibility	0.463	0.075	0.510	6.166	0.000 ***	0.220	4.542
Population of subdistrict	0.444	0.062	0.469	7.114	0.000 ***	0.348	2.876
Healthcare accessibility	−0.083	0.038	−0.129	−2.183	0.300 *	0.430	2.327
Length of metro lines	0.265	0.063	0.263	4.236	0.000 ***	0.392	2.554
Density of hotel and inn	0.434	0.103	0.326	4.217	0.000 ***	0.253	3.954
Density of metro lines	−0.172	0.056	−0.243	−3.046	0.003 **	0.237	4.216
Number of scenic spots	−0.137	0.045	−0.154	−3.060	0.003 **	0.596	1.677
Land use mix	0.138	0.052	0.127	2.649	0.009 **	0.657	1.522
Commuting accessibility	0.100	0.045	0.109	2.217	0.028 *	0.624	1.603

Dependent variable: infected population. Note. * $p < 0.05$, ** $p < 0.01$, *** $p < 0.001$.

In the empirical comparison of the OLS, GWR, and GTWR models using a reference case area, the results presented in Table 4 demonstrate that the GTWR model has a superior model fit compared to OLS and GWR. The R^2 value increased from 0.688 in OLS and 0.787 in GWR to 0.854 in GTWR, indicating that the non-stationary GTWR model better fits the data compared to the static OLS model. Additionally, AIC was computed for each model, and the one with the smallest value was selected as the best model, reflecting the least information loss compared to the true model [96,97]. In our study, the AIC value decreased from −391.54 and −392.81 in OLS and GWR, respectively, to −3610.16 in GTWR, suggesting that the inclusion of spatial and temporal information in the GTWR model significantly improved the explanatory power.

Table 4. Comparison results of OLS, GWR, and GTWR models.

	OLS	GWR	GTWR
R^2	0.688	0.787	0.854
Adjusted R^2	0.673	0.776	0.853
RSS	1.915	1.314	1.714
AICc [1]	−391.54	−392.81	−3610.16

[1] The Akaike information criterion (AIC) is an estimator of prediction error.

3.3. Spatial Variation of Estimated Coefficients

3.3.1. Spatial Distribution by Environmental Variables

We used the GTWR model to obtain average coefficients for selected variables and analyze their spatial variation among subdistricts or towns (Figure 7). Results were grouped into five categories based on natural breaks in the average coefficients. Metro line length had higher coefficients in the city-center area than other variables, while the density of Shanghai's metro lines had a negative impact on the central area and a transitional influence from negative to positive in the suburbs (Figure 7a,b). The quantity of scenic spots had a negative effect on infection cases, with decreasing coefficients towards the surrounding areas (Figure 7c). Hotel and inn density coefficients were mainly concentrated in distant suburbs adjacent to neighboring cities (Figure 7d). Healthcare facility accessibility positively impacted infected cases in the central area but had a negative impact outside the outer ring road. As accessibility decreased, the number of infected individuals increased in the central area while it decreased outside the outer ring road. (Figure 7e). Commuting accessibility negatively affected infected cases in the city center but positively affected them in the suburban areas (Figure 7f). Walking accessibility positively impacted the suburb ring, decreasing towards the suburbs and becoming negative in the distant suburbs (Figure 7g). Land use mixability and population had the strongest positive effects in downtown areas along the Huangpu River (Figure 7h,i).

3.3.2. Spatial Distribution by Temporal Scale

To examine differences in influence between March and July, we analyzed the coefficients of the nine most relevant factors identified in the stepwise regression over all five months, and the results are shown in Figures 8–11. In March, the township-level division population had the greatest influence on infected cases in the southeast part of Pudong and the east of Fengxian district, with declining impacts along the diagonal to the northwest. From April to June, the population coefficients for subdistricts or towns fluctuated significantly, with high and sub-high values traveling anti-clockwise to Pudong New Area and districts surrounding the Huangpu River, before shifting to the north in May with a decreasing influence from north to south (Figure 8). The impacts of metro line length varied regionally and temporally, with high positive values primarily in the northern riverside areas of Shanghai and central Chongming Island, but gradually shifting to central and then southern Shanghai, with the impact diminishing as the distance from high-value areas increased. The effect of metro line length on infected cases became negative after July, indicating a decreasing trend from south to north (Figure 9).

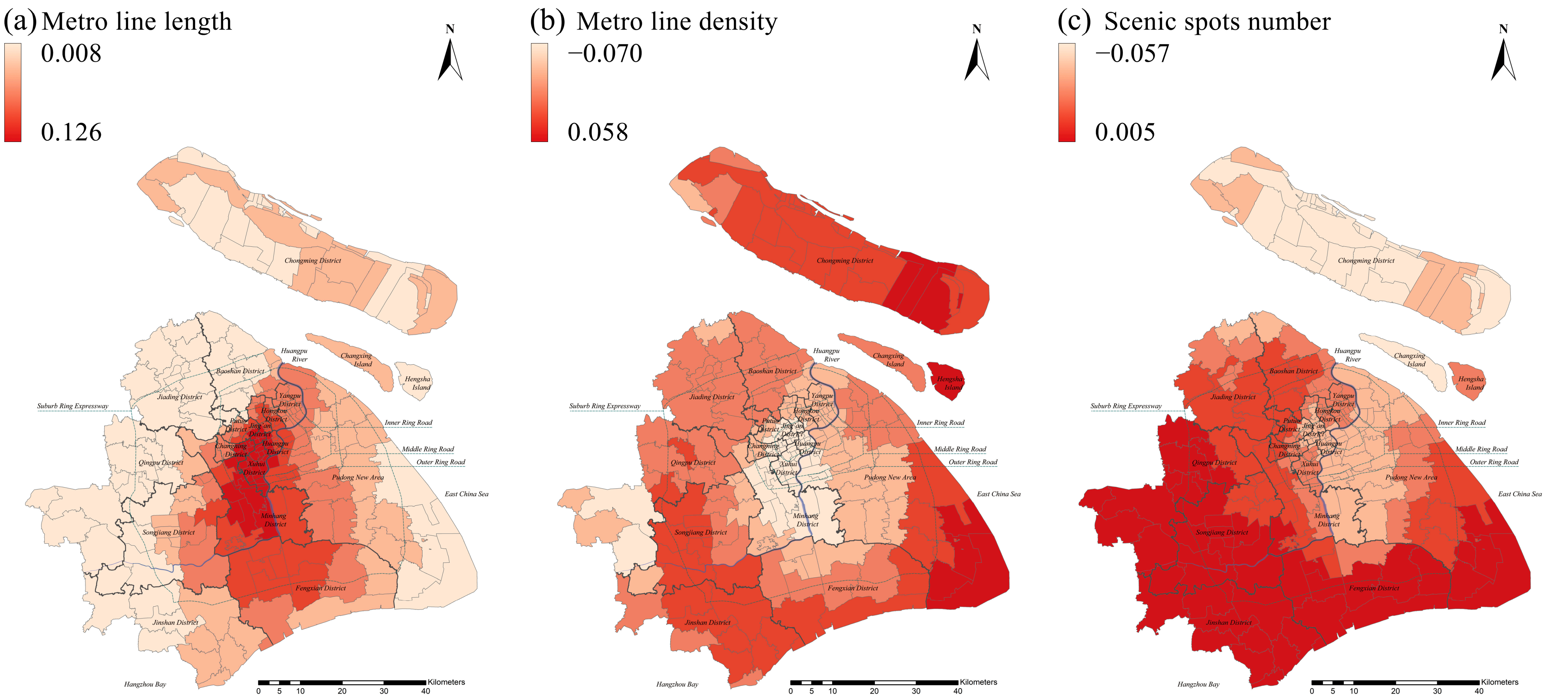

Figure 7. *Cont*.

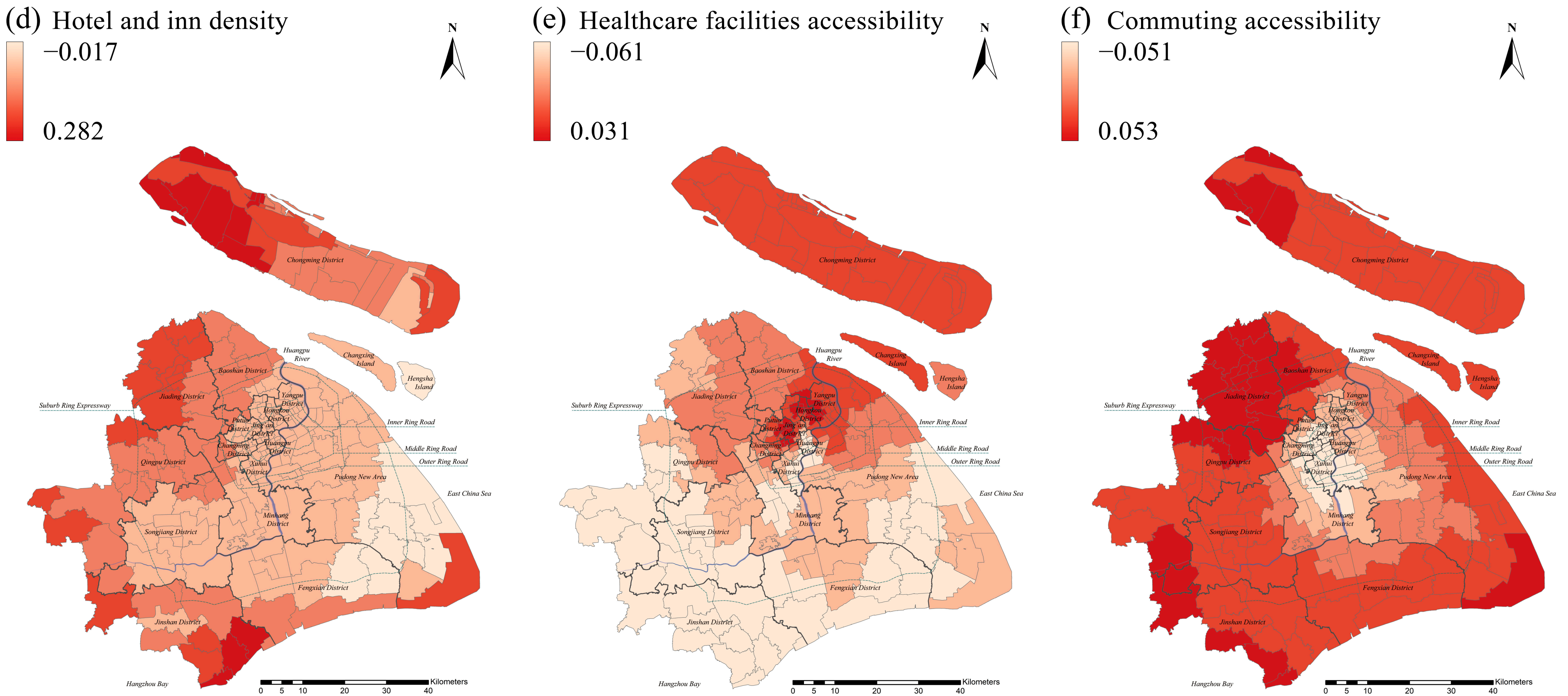

Figure 7. *Cont.*

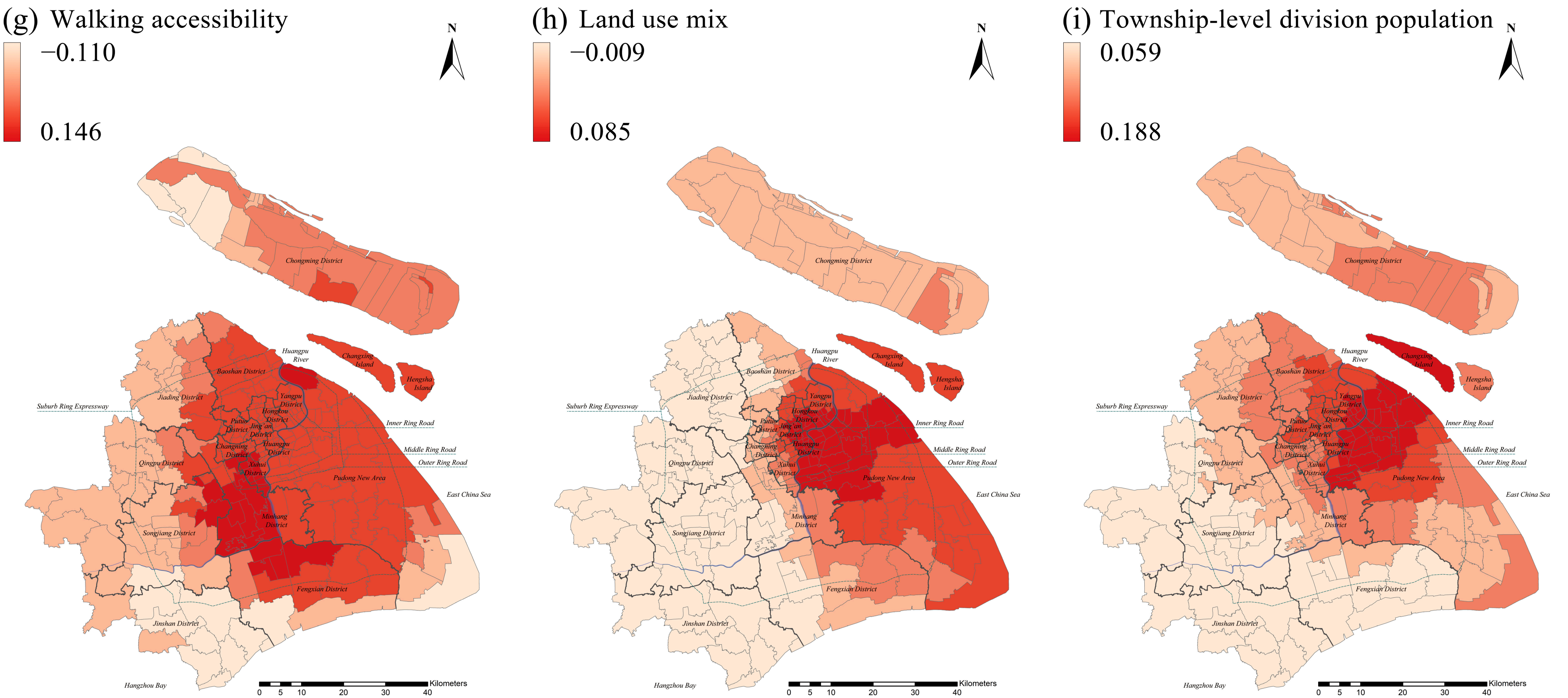

Figure 7. Spatial distribution of the average coefficients of GWR results for (**a**) metro line length; (**b**) metro line density; (**c**) scenic number; (**d**) hotel and inn density; (**e**) healthcare facilities accessibility; (**f**) commuting accessibility; (**g**) walking accessibility; (**h**) land use mix; (**i**) subdistrict population.

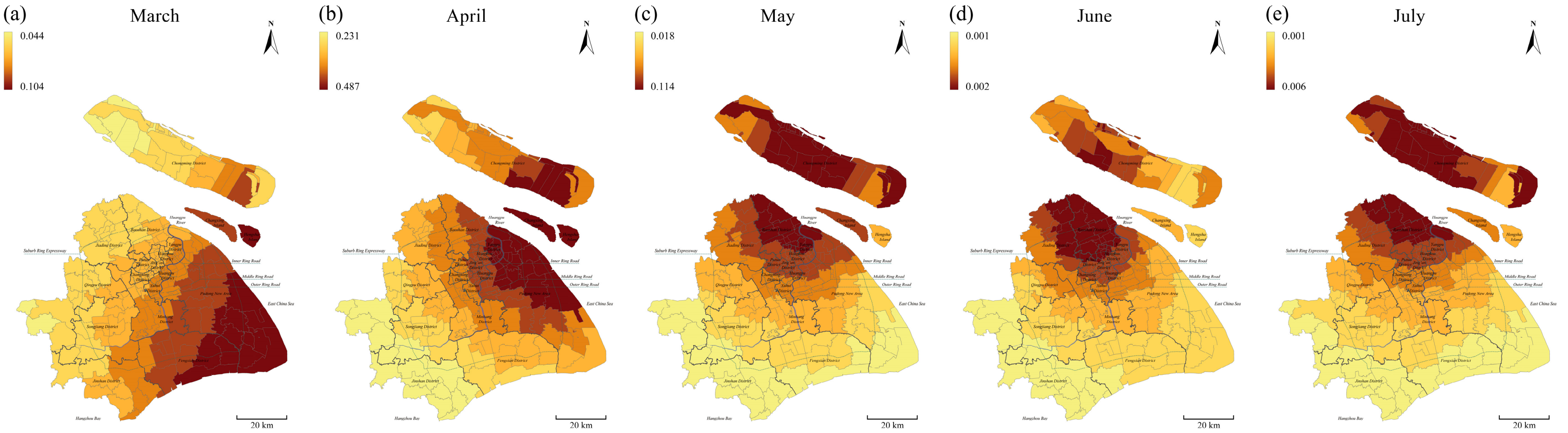

Figure 8. Spatial distribution of the average coefficients for township-level division population in five different months: (**a**) March; (**b**) April; (**c**) May; (**d**) June; (**e**) July.

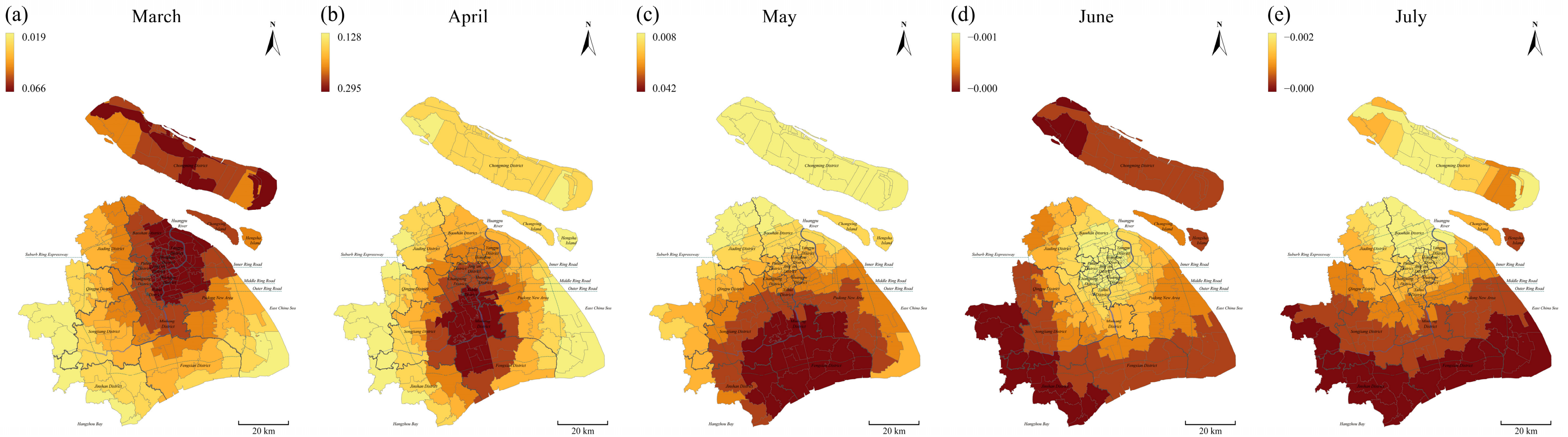

Figure 9. Spatial distribution of the average coefficients for metro line length in five different months: (**a**) March; (**b**) April; (**c**) May; (**d**) June; (**e**) July.

The effect of hotel and inn density on infected cases was positive during the first four months but largely negative by July, with the highest values in areas B (including some industrial zones in Jiading and Baoshan), C (including some industrial towns in Qingpu and Songjiang), and E (including some industrial towns and chemical industrial zones in Jinshan) from March to June, and in areas A (most of Chongming Island) and D (Lingang Special Area of Pudong New Area) in July (Figure 10). Figure 11 displays diverse geographical distribution patterns of walking accessibility coefficients over the five time periods. Positive coefficients were observed in April and May, partially negative coefficients were observed in March and July, and negative coefficients were observed in June. Negative impacts were primarily observed in some towns close to the provinces and a few towns in the north part of Chongming Island in March and July, while the rest of the area continued to demonstrate positive impacts. The highest values occurred mainly in the Puxi area in March and then throughout the Pudong New Area in July. In April and May, positive impacts and the highest values occurred in the center of Shanghai, decreasing in all directions, while in June, walking accessibility had a negative influence on infection rates throughout the city, with the highest and second-highest values seen in the southeast of Shanghai and values decreasing diagonally towards the northwest.

The findings depicted in Figures 8–11 illuminate the key BE factors associated with COVID-19 cases before, during, and after the lockdown in Shanghai. The significance of public transport connectivity, pedestrian accessibility, and population density aligns with Shanghai's aspiration to become a global economic center supported by a robust transportation network and activity centers. However, these urban development patterns may also facilitate disease transmission. The results emphasize the necessity for coordinated planning that integrates connectivity, density, and public health considerations.

3.3.3. Temporal Variation in Estimated Coefficients

The coefficients exhibit temporal and spatial variability, and we assessed their spatial patterns and magnitude of influence using eigenvalues, as presented in Table 5. Walk accessibility, land use mixability, hotel and inn density, and metro line length are positively associated with infected populations, while metro line density, shopping service density, work commuting accessibility, healthcare service accessibility, and scenic spot quantity are negatively associated. The township-level division population consistently shows a positive association. The effect of hotel and inn density, walking accessibility, and subdistrict or town population varies considerably over time, with a higher standard deviation of their average coefficients.

Table 5. Estimates of the GTWR model.

Variable	AVG	MIN	MAX	LQ	MED	UQ	SD
Intercept	−0.032	−0.197	0.011	−0.030	−0.015	0.000	0.049
Length of metro lines	0.065	−0.008	0.295	−0.001	0.021	0.065	0.097
Density of metro lines	−0.041	−0.162	0.007	−0.050	−0.018	0.000	0.056
Number of scenic spots	−0.032	−0.168	0.000	−0.053	−0.018	0.000	0.039
Hotel and inn density	0.107	−0.007	0.671	0.000	0.021	0.126	0.152
Healthcare facilities accessibility	−0.024	−0.181	0.002	−0.024	−0.002	−0.001	0.037
Commuting accessibility	−0.022	−0.005	0.149	0.000	0.005	0.018	0.036
Walking accessibility	0.111	−0.026	0.141	0.000	0.032	0.141	0.150
Land use mix	0.033	−0.014	0.203	−0.000	0.020	0.031	0.048
Population of Subdistrict or Town	0.114	0.001	0.487	0.003	0.070	0.100	0.153

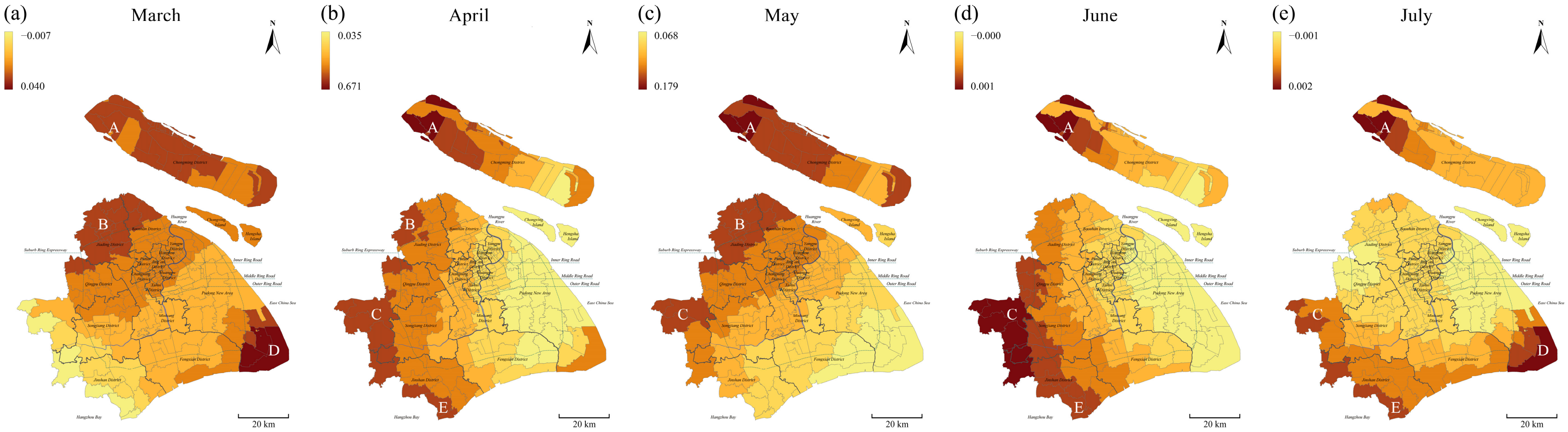

Figure 10. Spatial distribution of the average coefficients for hotel and inn density in five different months: (**a**) March; (**b**) April; (**c**) May; (**d**) June; (**e**) July.

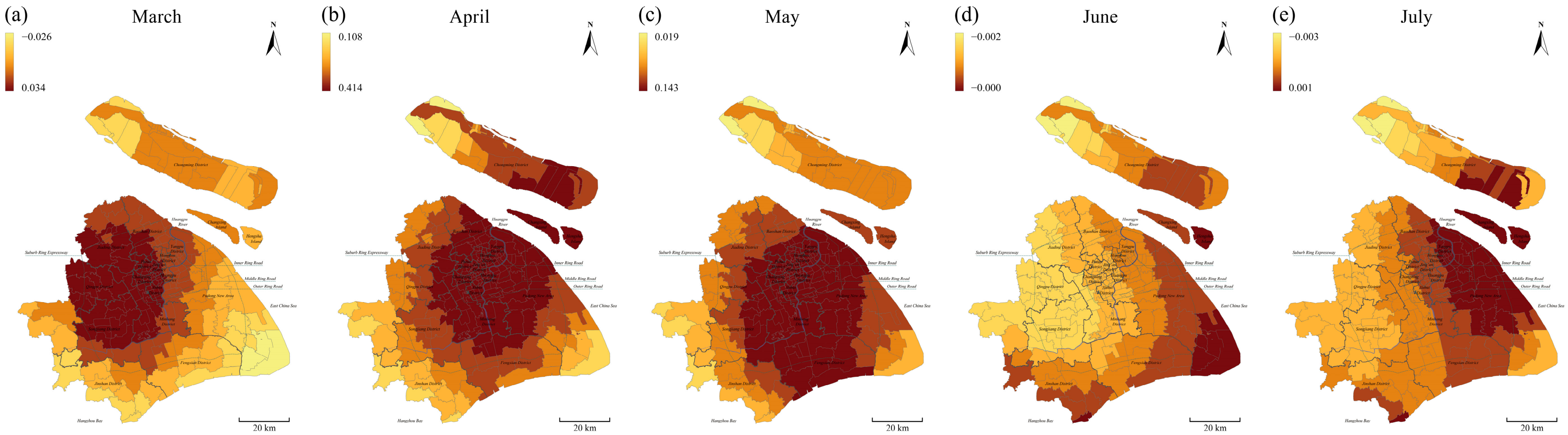

Figure 11. Spatial distribution of the average coefficients for walking accessibility in five different months: (**a**) March; (**b**) April; (**c**) May; (**d**) June; (**e**) July.

We computed the monthly average coefficient values of selected variables during the lockdown period, and these are presented in Figure 12 for different time periods, revealing two scenarios of coefficient growth trajectories from March to April. The coefficients of both scenarios continued to decline in their respective directions from April to May and from May through June, with coefficients stabilizing close to zero by June and July. We conclude that coefficient values increased in the first stage, decreased in the second stage, and finally stabilized in the third stage due to the influence of BE, which resulted in variables contributing to the spread of COVID-19 varying over time [19,62].

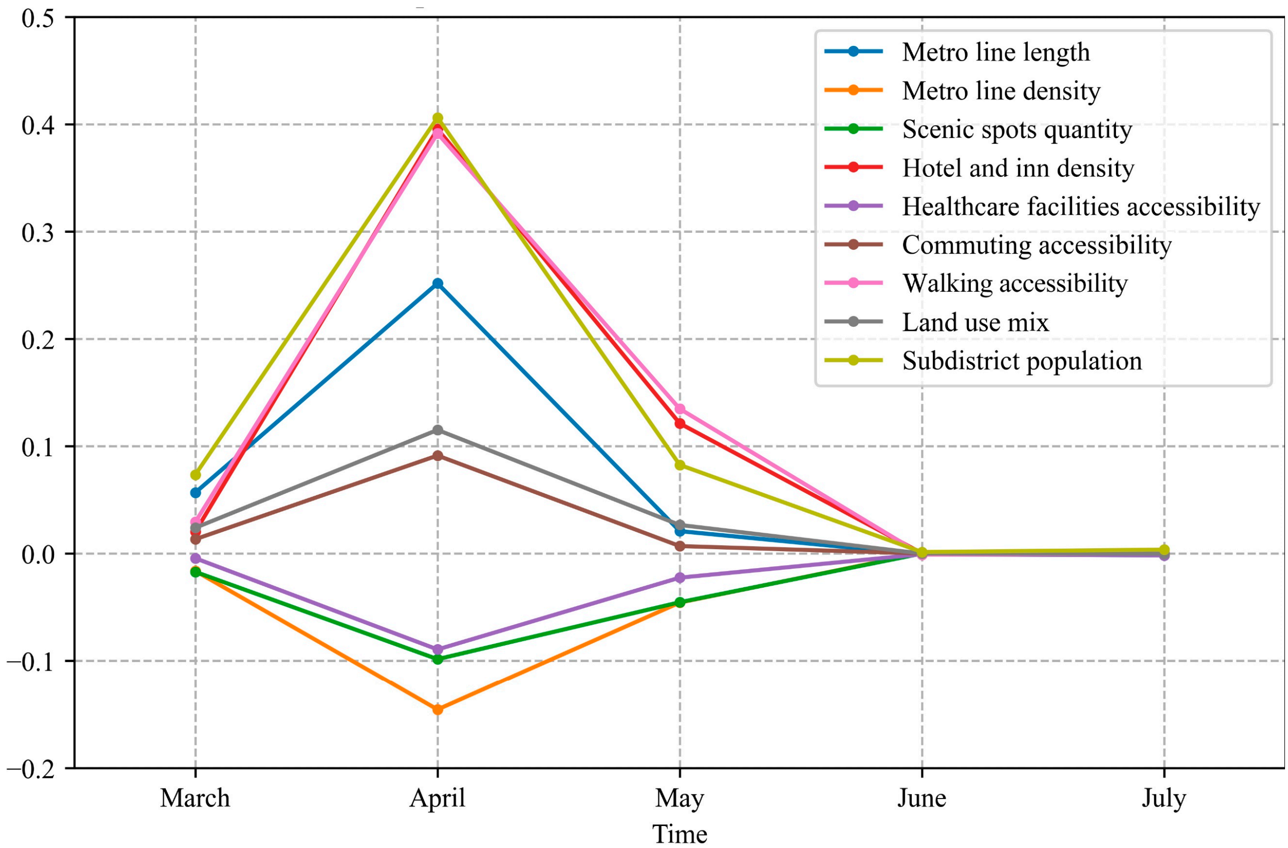

Figure 12. Temporal variation in the average monthly coefficients of selected variables from GTWR.

4. Discussion

We found that the association between BE variables and Omicron transmission varied spatially and temporally in Shanghai, with township-level division-based population, urban density, and destination accessibility identified as the most significant indicators.

4.1. Spatial Variability

This section focuses on spatial variations, using the average values for each township-level division with respect to time (Figure 7); temporal variations will be discussed in the following section.

4.1.1. Population, Transmission, and COVID-19 Policies

The influence of demographic characteristics on the transmission of COVID-19 is a significant research topic. Our findings support previous research on the positive correlation between population and COVID-19 prevalence [12,23,48]. However, contrasting findings have been reported for population density in previous studies conducted in Asia, such as Hong Kong [21] and cross-city studies in China [18,19], which may be attributed to the implementation of quarantine measures and regional restrictions in the studied areas. China's major cities, including Shenzhen, Guangzhou, Beijing, and Xi'an, experienced recurrent COVID-19 outbreaks in 2022, similar to Shanghai. Currently, it seems that the regional government's adherence to the widely endorsed Dynamic Zero COVID-19 Strategy, implemented since January 2020, has yielded more favorable outcomes in preventing COVID-19 transmission [98,99]. These governments implemented strict lockdown measures and extensive testing promptly following the reoccurrence of outbreaks [100], in contrast to Shanghai's looser strategies, such as community-based contact tracing and quarantine [101]. The rapid expansion of the Omicron variant outbreak in Shanghai can be attributed to the high transmissibility and potential immune-escape properties of Omicron BA.2.26, distinguishing it from previous localized SARS-CoV-2 outbreaks in China post-initial COVID-19 waves [102].

4.1.2. Mobility and Urban Transport System

Transportation is the most influential aspect of BE on the spread of infectious diseases, considering the mobility of humans across countries and cities and within cities. Shanghai is a globally connected city, with 30 to 40% of all international flights arriving in China since 2020 landing in the city, making infected tourists from other countries the origin of practically all cases before the city-wide lockdown [102,103]. As one of the primary modes of public transportation, the metro has been associated with high infection rates in districts where high patronage of metro stations was observed [11,24]. In our study, regions with more metro lines (e.g., Pudong New Area) and high-traffic interchange stations (e.g., Century Avenue, Longyang Road) had a higher risk of infection due to the denser metro network, which provides more intra-regional transportation interchanges and route alternatives, leading to additional opportunities for interpersonal interaction and the spread of disease in surrounding and peripheral regions.

4.1.3. COVID-19 Distribution and Accessibility Disparity

Accessibility to destinations, including healthcare facilities and workplaces, as well as overall walking accessibility, has a more substantial impact on the spread of COVID-19 than urban density and design, as shown in our regression results. Our findings indicate a positive link between walking accessibility in the city center and the risk of infection transmission, with the opposite result in the suburbs, suggesting that making suburban areas more accessible to walking may help reduce the spread of infection [104]. The correlation between walking accessibility and scenic spot distribution suggests that suburban areas with parks and open spaces can reduce stress, improve health, and lower the risk of infectious disease transmission by reducing public transportation use [61,105,106]. In contrast, outer suburbs with poor walking infrastructure and lower population densities may increase the reliance on public transportation and amplify the risk of infectious disease transmission [107,108]. Access to healthcare and traveling to work had opposing impacts on the spread of Omicron, with shorter commutes in highly populated locations associated with greater infection rates [109]. In contrast, lower infection rates in remote areas may be due to fewer people commuting during peak hours.

4.1.4. Epidemics and Land Mixing

Land use mix, as measured using POI mix, is positively related to the infected population, consistent with findings from previous studies in North America and Asia [21,30,110,111]. Downtown areas with high land use mixability tend to have a high population density and increased mobility, which can increase the likelihood of interaction between individuals and make it more challenging to track and suppress pandemics. However, our results are in contrast to those of Kan et al., who found that a more significant risk is associated with a larger proportion of green areas, higher median family income, and lower commercial land density in the vicinity of confirmed case dwellings [26]. Another study by Wali and Frank found that more mixed land use and greater pedestrian-oriented street connectivity correlate with lower COVID-19 hospitalization or fatality rates [112]. In Shanghai, parks with high levels of greenery have been found to potentially lower COVID-19 case rates, especially in densely populated urban areas [113], consistent with previous studies on COVID-19 and green space [15,106,114].

4.2. Temporal Dynamics

Local adaptive mechanisms and preventive measures are commonly employed to prevent and reduce the spread of infectious diseases [115]. Factors such as spatial attributes (BE variables) and human behavior (such as mobility, stress management, and adaptation) can contribute to the spread of COVID-19 and their dynamic and time-dependent nature must be considered when analyzing the spread of infectious diseases [116]. Previous studies have examined how different pandemic phases affect the influence of various variables, and the delay in adopting containment measures can account for regional variations in the number of COVID-19 cases [117]. However, the current literature lacks a comprehensive analysis of big data that considers both spatial and temporal factors. This study addresses this gap by utilizing multi-source big data at a subdistrict or town scale to investigate spatiotemporal correlations between BE variables and COVID-19 transmission. The findings highlight the importance of considering spatiotemporal variations when developing prevention measures and policies, given the variability of these factors over time and across regions.

4.2.1. Overall Temporal Variation in Built Environment Variables

A time series analysis of COVID-19 transmission in Shanghai revealed distinct variations in coefficients during each stage. The majority of incubation period instances occurred in the first stage, which preceded the Shanghai lockdown and saw a sharp increase in the total number of confirmed cases. The impact of individuals' movement and migration during their latent period in the second stage rapidly decreased and vanished. During the third stage, when the outbreak was under control, none of the coefficients changed with time. Figure 12 shows that the impacts of density were more pronounced during the early stages of COVID-19, which explains why urban centers and megacities were at the forefront of the disease's dissemination [38]. As the pandemic expanded, variables related to urban design dimensions, such as walking accessibility, commuter accessibility, and metro line length, became increasingly significant for the transmission of infection, while the influence of density-related variables diminished. We found that highly populated places are more susceptible to pandemic outbreaks, which supports previous research [38,118]. The distribution of confirmed infections in Shanghai followed the allocation of population density, with some other BE variables and indicators initially contributing to the incidence of infection and then degrading over time. The decreasing coefficient of the township-level division-based population from Pudong to the southwest of Puxi was attributed to the large population base and control measures limiting population mobility in the Pudong area.

4.2.2. Human Behaviors and Public Transportation

Aside from demography, individual mobility is a critical factor in determining the spread of infectious diseases [119]. Changes in habits and activities during the pandemic may have influenced the relationship between metro line length and infection rates over time, particularly in the context of mobility and transportation. Initially, increased public transportation usage may have led to higher infection rates and a positive association between the number of confirmed cases and metro line length, as observed in [19] and [108]. However, our findings reveal a subsequent negative correlation between metro line length and infection rates, likely due to the public's increased awareness of the dangers of using public transportation and their preference for private vehicles, walking, or cycling [120,121]. These behavioral changes suggest that the impact of transportation on pandemic transmission is not constant and may be influenced by various factors, such as public awareness and behavioral changes [120,122].

4.2.3. Temporal Variation in Accessibility

Walking accessibility, the most significant feature of the BE outside of sociodemographic factors, played a crucial role in the early stages of Omicron spread and became the most influential of all BE characteristics in the later stages of the lockdown. The accessibility of each township-level division followed the same pattern as the coefficient of pre-blockade walking accessibility in proportion to the number of infections. During the Shanghai lockdown, the effect of walking accessibility was most pronounced in the city center, likely due to higher population density and increased social interactions within residential areas. The movement restrictions implemented by the Shanghai government made human mobility within the same subdistrict or town stronger, supporting previous research showing that highly populated, walkable, and physically degraded areas are particularly susceptible to spreading COVID-19 [30]. However, in other months, high levels of walking accessibility were associated with a decreased infection rate, likely due to improved access to healthcare and public health services, as well as the usage of active transportation modes and the availability of open spaces and parks for outdoor exercise and recreation while maintaining social distance [123,124].

4.2.4. Hotel Density and COVID-19 Transmission

Our study highlights the spatial association between hotels and COVID-19 spread, which was previously ignored in research on isolation facilities for inbound tourists or close contacts [93]. We found that the configuration of urban industrial structures and the type of mid- to low-end hotels contributed to higher infection prevalence before, during, and after the lockdown. The industry concentration in Shanghai's suburbs has stimulated the growth of gross industrial output value and GDP, generating favorable benefits for Shanghai and increasing suburban employment and population [125]. However, the implementation and administration of pandemic prevention measures in small informal hotels, where most workers in the manufacturing and processing industries live, may be somewhat lax, raising the likelihood of disease transmission. In July, most areas within the suburban ring expressway were negatively impacted, possibly due to increased compliance with health rules, changes in population density, and fluctuations in the timing and intensity of the pandemic.

4.3. Limitations and Assumptions

This study has several limitations. Firstly, the asymptomatic infected and confirmed case data were obtained from the Shanghai Municipal Health Commission's daily reports. However, the tracking and estimation of asymptomatic cases were likely based on certain assumptions by the health authorities, as the full details are not publicly available. We have relied on the official reported figures in our analysis but caution that these asymptomatic case numbers may be subject to uncertainty.

Additionally, the BE variables remained stationary, while only the location data for infected population measurement varied temporally. Future studies should incorporate temporal details of BE variables, such as the opening hours of shopping venues and restaurant POIs and accessibility during weekdays, weekends, daytime, and nighttime. Additionally, contextual factors beyond the POI dataset from Amap, such as temperature, humidity, topography, policy implementation, and other control measures, should be considered in further research. Furthermore, population mobility at the community level and its impact on the spread of COVID-19 require further investigation.

4.4. Implications and Future Perspectives

In the context of the COVID-19 pandemic, our study explored the spatiotemporal impact of sociodemographic indicators and BE variables on COVID-19 spread. This analysis underscores the importance of evidence-based approaches in urban planning and public health policymaking, aligning with the objectives of SDG 3 for good health and well-being and SDG 11 for sustainable and resilient cities and communities. Our findings highlight the necessity for comprehensive public health strategies, including targeted quarantine measures, restrictions on international travel, and the promotion of active transportation modes such as walking and cycling. Urban policymakers and planners should prioritize understanding the spatial and temporal influences of BE variables on viral dissemination and foster resilience within cities.

The study suggests the significance of optimizing metro lines, improving ventilation design in metro systems and stations, and creating underground pedestrian routes while ensuring social equity from a public health perspective. Furthermore, targeted public health interventions, such as enhanced testing and contact tracing, should be implemented in areas with high population density and public transportation usage. Future research should focus on identifying susceptible settings and vulnerable demographics at smaller regional or individual levels. Policymakers should also consider the temporal dynamics of BE in disease transmission when formulating preventive measures against infectious diseases. This includes promoting walkable neighborhoods, efficiently allocating healthcare facilities, and integrating green spaces into urban design to enhance the resilience of cities.

5. Conclusions

The COVID-19 pandemic has highlighted gaps in understanding how BE factors influence disease transmission, especially considering spatial and temporal variations. This study aimed to address these gaps by investigating the spatiotemporal relationships between BE attributes and COVID-19 cases using multi-source urban data.

To capture localized variations, we focused the analysis at the township level across Shanghai during different phases of the Omicron outbreak and lockdown. The associations were analyzed using GTWR models and local coefficient time series clustering while accounting for spatial and temporal heterogeneity. The results show that the GTWR model accounted for over 85.4% of the variation and potential associated factors in COVID-19 cases. This novel approach allowed an assessment of how the impacts of BE measures like population density, transit accessibility, and land use mix evolve over time and space in the urban context. The results demonstrated significant spatiotemporal variability in the connections between BE factors and COVID-19 transmission. Regarding space, metro line length, walking accessibility, hotel density, and population, these showed consistently positive correlations with infection prevalence. Temporally, the relationships between accessibility, mobility, density, and COVID-19 cases shifted noticeably across pre-lockdown, lockdown, and post-lockdown stages.

In conclusion, this study underscores the significance of localized spatiotemporal analysis in comprehending the impact of the BE on the transmission of infectious diseases. The findings have practical implications for targeted urban planning and public health strategies tailored to the distinct spatial and temporal dynamics of various cities. Moreover, our research closely aligns with the United Nations' Sustainable Development Goals (SDGs), specifically SDG 3: Good Health and Well-Being, and SDG 11: Sustainable Cities and Communities. By investigating the spatiotemporal relationships between BE factors and COVID-19 transmission, our study contributes to understanding how urban planning and design interventions can enhance urban resilience against widespread infectious diseases. Policymakers and urban planners can utilize this knowledge to formulate customized strategies and interventions to mitigate the impact of future pandemics. Future research should consider integrating individual-level demographic and behavioral data at finer resolutions while incorporating additional contextual variables. This approach is essential for generating more accurate and nuanced insights. Furthermore, there is a need for further efforts to translate these findings into practical urban planning guidelines and public health protocols that are specifically tailored to local transmission profiles and community needs.

Supplementary Materials: The following supporting information can be downloaded at: https://www.mdpi.com/article/10.3390/ijgi12100390/s1, Table S1: Recent articles referring to the impacts of the built environment on COVID-19; Table S2: Descriptive statistics of dependent and explanatory variables. References [126–131] are cited in the supplementary materials.

Author Contributions: Conceptualization, Hao Huang; Methodology, Hao Huang; Investigation, Hao Huang; Formal analysis, Hao Huang; Writing—Original Draft, Hao Huang; Data Curation, Hao Huang; Visualization, Hao Huang, Haochen Shi; Writing—Review and Editing, Haochen Shi, Mirna Zordan, Jin Yeu Tsou; Validation, Mirna Zordan, Jin Yeu Tsou; Supervision, Siu Ming Lo, Jin Yeu Tsou. All authors have read and agreed to the published version of the manuscript.

Funding: This research received no external funding.

Data Availability Statement: The data that support the findings of this study are available from the first author upon reasonable request.

Conflicts of Interest: The authors declare no conflict of interest.

References

1. Ascher, K.; Marech, W.; Alexander, I. *The Works: Anatomy of a City*; Penguin Press: New York, NY, USA, 2005; ISBN 1-59420-071-8.
2. Santiago-Alarcon, D.; MacGregor-Fors, I. Cities and Pandemics: Urban Areas Are Ground Zero for the Transmission of Emerging Human Infectious Diseases. *J. Urban Ecol.* **2020**, *6*, juaa012. [CrossRef]
3. Liu, C.; Liu, Z.; Guan, C. The Impacts of the Built Environment on the Incidence Rate of COVID-19: A Case Study of King County, Washington. *Sustain. Cities Soc.* **2021**, *74*, 103144. [CrossRef] [PubMed]
4. Li, R.; Huang, Y. COVID-19 Pandemic and Minority Health Disparities in New York City: A Spatial and Temporal Perspective. *Environ. Plan. B Urban Anal. City Sci.* **2023**, *50*, 1194–1211. [CrossRef]
5. Nazroo, J.; Murray, K.; Taylor, H.; Bécares, L.; Field, Y.; Kapadia, D.; Rolston, Y. *Rapid Evidence Review: Inequalities in Relation to COVID-19 and Their Effects on London*; University of Manchester: London, UK; The Ubele Initiative: London, UK; University of Sussex: Brighton, UK, 2020.
6. Chakraborty, I.; Maity, P. COVID-19 Outbreak: Migration, Effects on Society, Global Environment and Prevention. *Sci. Total Environ.* **2020**, *728*, 138882. [CrossRef]
7. Sobczak, M.; Pawliczak, R. Factors That Affect the COVID-19 Pandemic in Summer 2022 Compared to Summer 2021. *Int. J. Environ. Res. Public Health* **2022**, *19*, 12561. [CrossRef]
8. Andreucci, M.B.; Marvuglia, A. Investigating, Implementing and Funding Regenerative Urban Design in a Post-COVID-19 Pandemic Built Environment: A Reading through Selected UN Sustainable Development Goals and the European Green Deal. In *Rethinking Sustainability towards a Regenerative Economy*; Andreucci, M.B., Marvuglia, A., Baltov, M., Hansen, P., Eds.; Future City; Springer International Publishing: Cham, Switzerland, 2021; Volume 15, pp. 395–413. ISBN 978-3-030-71818-3.
9. Fenner, R.; Cernev, T. The Implications of the COVID-19 Pandemic for Delivering the Sustainable Development Goals. *Futures* **2021**, *128*, 102726. [CrossRef]
10. Whyte, W.H. *The Social Life of Small Urban Spaces*; 7. print.; Project for Public Spaces: New York, NY, USA, 2010; ISBN 978-0-9706324-1-8.
11. Yip, T.L.; Huang, Y.; Liang, C. Built Environment and the Metropolitan Pandemic: Analysis of the COVID-19 Spread in Hong Kong. *Build. Environ.* **2021**, *188*, 107471. [CrossRef]
12. DiMaggio, C.; Klein, M.; Berry, C.; Frangos, S. Black/African American Communities Are at Highest Risk of COVID-19: Spatial Modeling of New York City ZIP Code–Level Testing Results. *Ann. Epidemiol.* **2020**, *51*, 7–13. [CrossRef]
13. Fortaleza, C.M.C.B.; Guimarães, R.B.; De Almeida, G.B.; Pronunciate, M.; Ferreira, C.P. Taking the Inner Route: Spatial and Demographic Factors Affecting Vulnerability to COVID-19 among 604 Cities from Inner São Paulo State, Brazil. *Epidemiol. Infect.* **2020**, *148*, e118. [CrossRef]
14. Dutta, I.; Basu, T.; Das, A. Spatial Analysis of COVID-19 Incidence and Its Determinants Using Spatial Modeling: A Study on India. *Environ. Chall.* **2021**, *4*, 100096. [CrossRef]
15. Klompmaker, J.O.; Hart, J.E.; Holland, I.; Sabath, M.B.; Wu, X.; Laden, F.; Dominici, F.; James, P. County-Level Exposures to Greenness and Associations with COVID-19 Incidence and Mortality in the United States. *Environ. Res.* **2021**, *199*, 111331. [CrossRef] [PubMed]
16. López-Gay, A.; Spijker, J.; Cole, H.V.S.; Marques, A.G.; Triguero-Mas, M.; Anguelovski, I.; Marí-Dell'Olmo, M.; Módenes, J.A.; Álamo-Junquera, D.; López-Gallego, F.; et al. Sociodemographic Determinants of Intraurban Variations in COVID-19 Incidence: The Case of Barcelona. *J. Epidemiol. Community Health* **2022**, *76*, 1–7. [CrossRef] [PubMed]
17. Md Iderus, N.H.; Lakha Singh, S.S.; Mohd Ghazali, S.; Yoon Ling, C.; Cia Vei, T.; Md Zamri, A.S.S.; Ahmad Jaafar, N.; Ruslan, Q.; Ahmad Jaghfar, N.H.; Gill, B.S. Correlation between Population Density and COVID-19 Cases during the Third Wave in Malaysia: Effect of the Delta Variant. *Int. J. Environ. Res. Public Health* **2022**, *19*, 7439. [CrossRef] [PubMed]
18. Zhang, H.; Liu, Y.; Chen, F.; Mi, B.; Zeng, L.; Pei, L. The Effect of Sociodemographic Factors on COVID-19 Incidence of 342 Cities in China: A Geographically Weighted Regression Model Analysis. *BMC Infect. Dis.* **2021**, *21*, 428. [CrossRef] [PubMed]
19. Liu, L. Emerging Study on the Transmission of the Novel Coronavirus (COVID-19) from Urban Perspective: Evidence from China. *Cities* **2020**, *103*, 102759. [CrossRef] [PubMed]
20. Barak, N.; Sommer, U.; Mualam, N. Urban Attributes and the Spread of COVID-19: The Effects of Density, Compliance and Socio-Political Factors in Israel. *Sci. Total Environ.* **2021**, *793*, 148626. [CrossRef]

21. Huang, J.; Kwan, M.-P.; Kan, Z.; Wong, M.; Kwok, C.; Yu, X. Investigating the Relationship between the Built Environment and Relative Risk of COVID-19 in Hong Kong. *IJGI* **2020**, *9*, 624. [CrossRef]
22. Li, X.; Zhou, L.; Jia, T.; Peng, R.; Fu, X.; Zou, Y. Associating COVID-19 Severity with Urban Factors: A Case Study of Wuhan. *Int. J. Environ. Res. Public Health* **2020**, *17*, 6712. [CrossRef]
23. You, H.; Wu, X.; Guo, X. Distribution of COVID-19 Morbidity Rate in Association with Social and Economic Factors in Wuhan, China: Implications for Urban Development. *Int. J. Environ. Res. Public Health* **2020**, *17*, 3417. [CrossRef]
24. Li, B.; Peng, Y.; He, H.; Wang, M.; Feng, T. Built Environment and Early Infection of COVID-19 in Urban Districts: A Case Study of Huangzhou. *Sustain. Cities Soc.* **2021**, *66*, 102685. [CrossRef]
25. Ma, S.; Li, S.; Zhang, J. Diverse and Nonlinear Influences of Built Environment Factors on COVID-19 Spread across Townships in China at Its Initial Stage. *Sci. Rep.* **2021**, *11*, 12415. [CrossRef] [PubMed]
26. Kan, Z.; Kwan, M.-P.; Wong, M.S.; Huang, J.; Liu, D. Identifying the Space-Time Patterns of COVID-19 Risk and Their Associations with Different Built Environment Features in Hong Kong. *Sci. Total Environ.* **2021**, *772*, 145379. [CrossRef]
27. Schmiege, D.; Haselhoff, T.; Ahmed, S.; Anastasiou, O.E.; Moebus, S. Associations Between Built Environment Factors and SARS-CoV-2 Infections at the Neighbourhood Level in a Metropolitan Area in Germany. *J. Urban Health* **2023**, *100*, 40–50. [CrossRef] [PubMed]
28. Hu, T.; Yue, H.; Wang, C.; She, B.; Ye, X.; Liu, R.; Zhu, X.; Guan, W.W.; Bao, S. Racial Segregation, Testing Site Access, and COVID-19 Incidence Rate in Massachusetts, USA. *Int. J. Environ. Res. Public Health* **2020**, *17*, 9528. [CrossRef] [PubMed]
29. Guan, C.; Tan, J.; Hall, B.; Liu, C.; Li, Y.; Cai, Z. The Effect of the Built Environment on the COVID-19 Pandemic at the Initial Stage: A County-Level Study of the USA. *Sustainability* **2022**, *14*, 3417. [CrossRef]
30. Nguyen, Q.C.; Huang, Y.; Kumar, A.; Duan, H.; Keralis, J.M.; Dwivedi, P.; Meng, H.-W.; Brunisholz, K.D.; Jay, J.; Javanmardi, M.; et al. Using 164 Million Google Street View Images to Derive Built Environment Predictors of COVID-19 Cases. *Int. J. Environ. Res. Public Health* **2020**, *17*, 6359. [CrossRef]
31. Li, S.; Ma, S.; Zhang, J. Association of Built Environment Attributes with the Spread of COVID-19 at Its Initial Stage in China. *Sustain. Cities Soc.* **2021**, *67*, 102752. [CrossRef]
32. Wang, J.; Wu, X.; Wang, R.; He, D.; Li, D.; Yang, L.; Yang, Y.; Lu, Y. Review of Associations between Built Environment Characteristics and Severe Acute Respiratory Syndrome Coronavirus 2 Infection Risk. *Int. J. Environ. Res. Public Health* **2021**, *18*, 7561. [CrossRef]
33. Wang, S.; Liu, Y.; Lam, J.; Kwan, M.-P. The Effects of the Built Environment on the General Health, Physical Activity and Obesity of Adults in Queensland, Australia. *Spat. Spatio-Temporal Epidemiol.* **2021**, *39*, 100456. [CrossRef]
34. Xiao, Y.; Chen, S.; Miao, S.; Yu, Y. Exploring the Mediating Effect of Physical Activities on Built Environment and Obesity for Elderly People: Evidence from Shanghai, China. *Front. Public Health* **2022**, *10*, 853292. [CrossRef]
35. Ewing, R.; Cervero, R. Travel and the Built Environment: A Meta-Analysis. *J. Am. Plan. Assoc.* **2010**, *76*, 265–294. [CrossRef]
36. Witten, K.; Blakely, T.; Bagheri, N.; Badland, H.; Ivory, V.; Pearce, J.; Mavoa, S.; Hinckson, E.; Schofield, G. Neighborhood Built Environment and Transport and Leisure Physical Activity: Findings Using Objective Exposure and Outcome Measures in New Zealand. *Environ. Health Perspect.* **2012**, *120*, 971–977. [CrossRef]
37. Liu, L.; Zhang, M.; Xu, T. A Conceptual Framework and Implementation Tool for Land Use Planning for Corridor Transit Oriented Development. *Cities* **2020**, *107*, 102939. [CrossRef]
38. Carozzi, F. Urban Density and COVID-19. *SSRN J.* **2020**. [CrossRef]
39. Rahman, M.H.; Zafri, N.M.; Ashik, F.; Waliullah, M. Gis-Based Spatial Modeling to Identify Factors Affecting COVID-19 Incidence Rates in Bangladesh. *SSRN J.* **2020**. [CrossRef]
40. Kim, B.; Rundle, A.G.; Goodwin, A.T.S.; Morrison, C.N.; Branas, C.C.; El-Sadr, W.; Duncan, D.T. COVID-19 Testing, Case, and Death Rates and Spatial Socio-Demographics in New York City: An Ecological Analysis as of June 2020. *Health Place* **2021**, *68*, 102539. [CrossRef]
41. Yang, T.-C.; Kim, S.; Zhao, Y.; Choi, S.E. Examining Spatial Inequality in COVID-19 Positivity Rates across New York City ZIP Codes. *Health Place* **2021**, *69*, 102574. [CrossRef]
42. Ma, S.; Li, S.; Zhang, J. The Spread of COVID-19 in China at Its Initial Stage: A Township-Level Analysis in Association with the Built Environment. *SSRN J.* **2020**. [CrossRef]
43. Scarpone, C.; Brinkmann, S.T.; Große, T.; Sonnenwald, D.; Fuchs, M.; Walker, B.B. A Multimethod Approach for County-Scale Geospatial Analysis of Emerging Infectious Diseases: A Cross-Sectional Case Study of COVID-19 Incidence in Germany. *Int. J. Health Geogr.* **2020**, *19*, 32. [CrossRef]
44. Fischer, M.M. Spatial Analysis in Geography. In *International Encyclopedia of the Social & Behavioral Sciences*; Elsevier: Amsterdam, The Netherlands, 2015; pp. 94–99. ISBN 978-0-08-097087-5.
45. Lin, Y.; Yang, B.; Cobey, S.; Lau, E.H.Y.; Adam, D.C.; Wong, J.Y.; Bond, H.S.; Cheung, J.K.; Ho, F.; Gao, H.; et al. Incorporating Temporal Distribution of Population-Level Viral Load Enables Real-Time Estimation of COVID-19 Transmission. *Nat. Commun.* **2022**, *13*, 1155. [CrossRef]
46. Chen, Y.; Chen, M.; Huang, B.; Wu, C.; Shi, W. Modeling the Spatiotemporal Association Between COVID-19 Transmission and Population Mobility Using Geographically and Temporally Weighted Regression. *GeoHealth* **2021**, *5*, e2021GH000402. [CrossRef]
47. Ling, L.; Qian, X.; Guo, S.; Ukkusuri, S.V. Spatiotemporal Impacts of Human Activities and Socio-Demographics during the COVID-19 Outbreak in the US. *BMC Public Health* **2022**, *22*, 1466. [CrossRef]

48. Sy, K.T.L.; White, L.F.; Nichols, B.E. Population Density and Basic Reproductive Number of COVID-19 across United States Counties. *PLoS ONE* **2021**, *16*, e0249271. [CrossRef]
49. Credit, K. Neighbourhood Inequity: Exploring the Factors Underlying Racial and Ethnic Disparities in COVID-19 Testing and Infection Rates Using ZIP Code Data in Chicago and New York. *Reg. Sci. Policy Pract.* **2020**, *12*, 1249–1271. [CrossRef]
50. Wong, D.W.S.; Li, Y. Spreading of COVID-19: Density Matters. *PLoS ONE* **2020**, *15*, e0242398. [CrossRef]
51. Teller, J. Urban Density and COVID-19: Towards an Adaptive Approach. *Build. Cities* **2021**, *2*, 150–165. [CrossRef]
52. Chung, C.K.L.; Xu, J.; Zhang, M. Geographies of COVID-19: How Space and Virus Shape Each Other. *Asian Geogr.* **2020**, *37*, 99–116. [CrossRef]
53. He, Q.; He, W.; Song, Y.; Wu, J.; Yin, C.; Mou, Y. The Impact of Urban Growth Patterns on Urban Vitality in Newly Built-Up Areas Based on an Association Rules Analysis Using Geographical 'Big Data'. *Land Use Policy* **2018**, *78*, 726–738. [CrossRef]
54. Wu, C.; Ye, X.; Ren, F.; Du, Q. Check-in Behaviour and Spatio-Temporal Vibrancy: An Exploratory Analysis in Shenzhen, China. *Cities* **2018**, *77*, 104–116. [CrossRef]
55. Wang, J.; McDonald, N.; Cochran, A.L.; Oluyede, L.; Wolfe, M.; Prunkl, L. Health Care Visits during the COVID-19 Pandemic: A Spatial and Temporal Analysis of Mobile Device Data. *Health Place* **2021**, *72*, 102679. [CrossRef]
56. Peng, J.; Liu, H.; Tang, J.; Peng, C.; Yang, X.; Deng, M.; Xu, Y. Exploring Crowd Travel Demands Based on the Characteristics of Spatiotemporal Interaction between Urban Functional Zones. *IJGI* **2023**, *12*, 225. [CrossRef]
57. Qu, J.; Zhang, J. Validating Mobile Designs with Agile Testing in China: Based on Baidu Map for Mobile. In *Design, User Experience, and Usability: Design Thinking and Methods*; Marcus, A., Ed.; Lecture Notes in Computer Science; Springer International Publishing: Cham, Switzerland, 2016; Volume 9746, pp. 491–498. ISBN 978-3-319-40408-0.
58. Dong, G.; Li, R.; Wu, H.; Chen, W.; Huang, W.; Zhang, H. Browsing Behavior Modeling and Browsing Interest Extraction in the Trajectories on Web Map Service Platforms. *Expert Syst. Appl.* **2022**, *195*, 116590. [CrossRef]
59. Wachs, M.; Kumagai, T.G. Physical Accessibility as a Social Indicator. *Socio-Econ. Plan. Sci.* **1973**, *7*, 437–456. [CrossRef]
60. Higgins, C.; Palm, M.; DeJohn, A.; Xi, L.; Vaughan, J.; Farber, S.; Widener, M.; Miller, E. Calculating Place-Based Transit Accessibility: Methods, Tools and Algorithmic Dependence. *JTLU* **2022**, *15*, 95–116. [CrossRef]
61. Khahro, S.H.; Talpur, M.A.H.; Bhellar, M.G.; Das, G.; Shaikh, H.; Sultan, B. GIS-Based Sustainable Accessibility Mapping of Urban Parks: Evidence from the Second Largest Settlement of Sindh, Pakistan. *Sustainability* **2023**, *15*, 6228. [CrossRef]
62. Talpur, M.A.H.; Khahro, S.H.; Ali, T.H.; Waseem, H.B.; Napiah, M. Computing Travel Impendences Using Trip Generation Regression Model: A Phenomenon of Travel Decision-Making Process of Rural Households. *Environ. Dev. Sustain.* **2023**, *25*, 5973–5996. [CrossRef]
63. Cooper, C.H.V.; Chiaradia, A.J.F. sDNA: 3-d Spatial Network Analysis for GIS, CAD, Command Line & Python. *SoftwareX* **2020**, *12*, 100525. [CrossRef]
64. Shi, H.; Zhao, M.; Simth, D.A.; Chi, B. Behind the Land Use Mix: Measuring the Functional Compatibility in Urban and Sub-Urban Areas of China. *Land* **2021**, *11*, 2. [CrossRef]
65. Carver, S.J. Integrating Multi-Criteria Evaluation with Geographical Information Systems. *Int. J. Geogr. Inf. Syst.* **1991**, *5*, 321–339. [CrossRef]
66. Mazziotta, M.; Pareto, A. Methods for Constructing Composite Indices: One for All or All for One. *Riv. Ital. Econ. Demogr. Stat.* **2013**, *67*, 67–80.
67. Libório, M.P.; Diniz, A.M.A.; Rabiei-Dastjerd, H.; Martinuci, O.D.S.; Martins, C.A.P.D.S.; Ekel, P.I. A Decision Framework for Identifying Methods to Construct Stable Composite Indicators That Capture the Concept of Multidimensional Social Phenomena: The Case of Social Exclusion. *Sustainability* **2023**, *15*, 6171. [CrossRef]
68. Thompson, B. Stepwise Regression and Stepwise Discriminant Analysis Need Not Apply Here: A Guidelines Editorial. *Educ. Psychol. Meas.* **1995**, *55*, 525–534. [CrossRef]
69. Saltelli, A.; Ratto, M.; Tarantola, S.; Campolongo, F. Sensitivity Analysis Practices: Strategies for Model-Based Inference. *Reliab. Eng. Syst. Saf.* **2006**, *91*, 1109–1125. [CrossRef]
70. Wang, M.; Wright, J.; Brownlee, A.; Buswell, R. A Comparison of Approaches to Stepwise Regression on Variables Sensitivities in Building Simulation and Analysis. *Energy Build.* **2016**, *127*, 313–326. [CrossRef]
71. Whittingham, M.J.; Stephens, P.A.; Bradbury, R.B.; Freckleton, R.P. Why Do We Still Use Stepwise Modelling in Ecology and Behaviour? Stepwise Modelling in Ecology and Behaviour. *J. Anim. Ecol.* **2006**, *75*, 1182–1189. [CrossRef]
72. Sisman, S.; Aydinoglu, A.C. A Modelling Approach with Geographically Weighted Regression Methods for Determining Geographic Variation and Influencing Factors in Housing Price: A Case in Istanbul. *Land Use Policy* **2022**, *119*, 106183. [CrossRef]
73. Craney, T.A.; Surles, J.G. Model-Dependent Variance Inflation Factor Cutoff Values. *Qual. Eng.* **2002**, *14*, 391–403. [CrossRef]
74. Christopher, J.; Kutner, M.H.; Li, W.; Neter, J.; Kutner, M. *Applied Linear Statistical Models*, 5th ed.; Kutner, M.H., Ed.; The McGraw-Hill/Irwin Series Operations and Decision Sciences; McGraw-Hill Irwin: Boston, UK, 2005; ISBN 978-0-07-238688-2.
75. Miles, J. Tolerance and Variance Inflation Factor. In *Wiley StatsRef: Statistics Reference Online*; Balakrishnan, N., Colton, T., Everitt, B., Piegorsch, W., Ruggeri, F., Teugels, J.L., Eds.; Wiley: Hoboken, NJ, USA, 2014; ISBN 978-1-118-44511-2.
76. An, R.; Wu, Z.; Tong, Z.; Qin, S.; Zhu, Y.; Liu, Y. How the Built Environment Promotes Public Transportation in Wuhan: A Multiscale Geographically Weighted Regression Analysis. *Travel Behav. Soc.* **2022**, *29*, 186–199. [CrossRef]
77. Huang, B.; Wu, B.; Barry, M. Geographically and Temporally Weighted Regression for Modeling Spatio-Temporal Variation in House Prices. *Int. J. Geogr. Inf. Sci.* **2010**, *24*, 383–401. [CrossRef]

78. Ma, X.; Zhang, J.; Ding, C.; Wang, Y. A Geographically and Temporally Weighted Regression Model to Explore the Spatiotemporal Influence of Built Environment on Transit Ridership. *Comput. Environ. Urban Syst.* **2018**, *70*, 113–124. [CrossRef]
79. Chu, H.-J.; Huang, B.; Lin, C.-Y. Modeling the Spatio-Temporal Heterogeneity in the PM10-PM2.5 Relationship. *Atmos. Environ.* **2015**, *102*, 176–182. [CrossRef]
80. Fu, X.; Zhai, W. Examining the Spatial and Temporal Relationship between Social Vulnerability and Stay-at-Home Behaviors in New York City during the COVID-19 Pandemic. *Sustain. Cities Soc.* **2021**, *67*, 102757. [CrossRef]
81. Chen, L.; Zhao, L.; Xiao, Y.; Lu, Y. Investigating the Spatiotemporal Pattern between the Built Environment and Urban Vibrancy Using Big Data in Shenzhen, China. *Comput. Environ. Urban Syst.* **2022**, *95*, 101827. [CrossRef]
82. Fotheringham, A.S.; Brunsdon, C.; Charlton, M. *Geographically Weighted Regression: The Analysis of Spatially Varying Relationships*; Wiley: Chichester, UK; Hoboken, NJ, USA, 2002; ISBN 978-0-471-49616-8.
83. Alcântara, E.; Mantovani, J.; Rotta, L.; Park, E.; Rodrigues, T.; Campos Carvalho, F.; Roberto Souza Filho, C. Investigating Spatiotemporal Patterns of the COVID-19 in São Paulo State, Brazil. *Geospat. Health* **2020**, *15*, 925. [CrossRef]
84. Ghosh, P.; Cartone, A. A Spatio-temporal Analysis of COVID-19 Outbreak in Italy. *Reg. Sci. Policy Pract.* **2020**, *12*, 1047–1062. [CrossRef]
85. Moran, P.A. The Interpretation of Statistical Maps. *J. R. Stat. Soc. Ser. B (Methodol.)* **1948**, *10*, 243–251. [CrossRef]
86. Anselin, L. The Moran Scatterplot as an ESDA Tool to Assess Local Instability in Spatial Association. In *Spatial Analytical Perspectives on GIS*; Routledge: London, UK, 2019; pp. 111–126.
87. Anselin, L. *Spatial Econometrics: Methods and Models*; Springer Science & Business Media: Berlin, Germany, 1988; Volume 4, ISBN 90-247-3735-4.
88. Anselin, L. Local Indicators of Spatial Association—LISA. *Geogr. Anal.* **1995**, *27*, 93–115. [CrossRef]
89. Scardaccione, G.; Scorza, F.; Casas, G.L.; Murgante, B. Spatial Autocorrelation Analysis for the Evaluation of Migration Flows: The Italian Case. In Proceedings of the Computational Science and Its Applications–ICCSA 2010: International Conference, Fukuoka, Japan, 23–26 March 2010; Part I 10. Springer: Berlin/Heidelberg, Germany, 2010; pp. 62–76.
90. Leung, Y.; Mei, C.-L.; Zhang, W.-X. Testing for Spatial Autocorrelation among the Residuals of the Geographically Weighted Regression. *Environ. Plan. A* **2000**, *32*, 871–890. [CrossRef]
91. Chen, Y. Spatial Autocorrelation Approaches to Testing Residuals from Least Squares Regression. *PLoS ONE* **2016**, *11*, e0146865. [CrossRef]
92. Ma, X.; Ji, Y.; Yuan, Y.; Van Oort, N.; Jin, Y.; Hoogendoorn, S. A Comparison in Travel Patterns and Determinants of User Demand between Docked and Dockless Bike-Sharing Systems Using Multi-Sourced Data. *Transp. Res. Part A Policy Pract.* **2020**, *139*, 148–173. [CrossRef]
93. Ma, J.; Zhu, H.; Li, P.; Liu, C.; Li, F.; Luo, Z.; Zhang, M.; Li, L. Spatial Patterns of the Spread of COVID-19 in Singapore and the Influencing Factors. *IJGI* **2022**, *11*, 152. [CrossRef]
94. Zhang, L.; Ma, Z.; Guo, L. An Evaluation of Spatial Autocorrelation and Heterogeneity in the Residuals of Six Regression Models. *For. Sci.* **2009**, *55*, 533–548.
95. Griffith, D.; Chun, Y. Evaluating Eigenvector Spatial Filter Corrections for Omitted Georeferenced Variables. *Econometrics* **2016**, *4*, 29. [CrossRef]
96. Burnham, K.P.; Anderson, D.R.; Huyvaert, K.P. AIC Model Selection and Multimodel Inference in Behavioral Ecology: Some Background, Observations, and Comparisons. *Behav. Ecol. Sociobiol.* **2011**, *65*, 23–35. [CrossRef]
97. Baguley, T. *Serious Stats: A Guide to Advanced Statistics for the Behavioral Sciences*; Palgrave Macmillan: Basingstoke, UK; New York, NY, USA, 2012; ISBN 978-0-230-57717-6.
98. Liu, J.; Liu, M.; Liang, W.; School of Public Health, Peking University, Beijing, China; Vanke School of Public Health, Tsinghua University, Beijing, China; Institute for Healthy China, Tsinghua University, Beijing, China. The Dynamic COVID-Zero Strategy in China. *China CDC Wkly.* **2022**, *4*, 74–75. [CrossRef]
99. Zhang, X.; Zhang, W.; Chen, S. Shanghai's Life-Saving Efforts against the Current Omicron Wave of the COVID-19 Pandemic. *Lancet* **2022**, *399*, 2011–2012. [CrossRef] [PubMed]
100. Zhou, Y.; Jiang, H.; Wang, Q.; Yang, M.; Chen, Y.; Jiang, Q. Use of Contact Tracing, Isolation, and Mass Testing to Control Transmission of COVID-19 in China. *BMJ* **2021**, *375*, n2330. [CrossRef]
101. Cheshmehzangi, A.; Zou, T.; Su, Z. Commentary: China's Zero-COVID Approach Depends on Shanghai's Outbreak Control. *Front. Public Health* **2022**, *10*, 912992. [CrossRef]
102. Chen, Z.; Deng, X.; Fang, L.; Sun, K.; Wu, Y.; Che, T.; Zou, J.; Cai, J.; Liu, H.; Wang, Y.; et al. Epidemiological Characteristics and Transmission Dynamics of the Outbreak Caused by the SARS-CoV-2 Omicron Variant in Shanghai, China: A Descriptive Study. *Lancet Reg. Health—West. Pac.* **2022**, *29*, 100592. [CrossRef]
103. Cai, J.; Deng, X.; Yang, J.; Sun, K.; Liu, H.; Chen, Z.; Peng, C.; Chen, X.; Wu, Q.; Zou, J.; et al. Modeling Transmission of SARS-CoV-2 Omicron in China. *Nat. Med.* **2022**, *28*, 1468–1475. [CrossRef]
104. Baobeid, A.; Koç, M.; Al-Ghamdi, S.G. Walkability and Its Relationships With Health, Sustainability, and Livability: Elements of Physical Environment and Evaluation Frameworks. *Front. Built Environ.* **2021**, *7*, 721218. [CrossRef]
105. Lee, K.O.; Mai, K.M.; Park, S. Green Space Accessibility Helps Buffer Declined Mental Health during the COVID-19 Pandemic: Evidence from Big Data in the United Kingdom. *Nat. Ment. Health* **2023**, *1*, 124–134. [CrossRef]
106. Jiang, B.; Yang, Y.; Chen, L.; Liu, X.; Wu, X.; Chen, B.; Webster, C.; Sullivan, W.C.; Larsen, L.; Wang, J.; et al. Green Spaces, Especially Nearby Forest, May Reduce the SARS-CoV-2 Infection Rate: A Nationwide Study in the United States. *Landsc. Urban Plan.* **2022**, *228*, 104583. [CrossRef]

107. Almagro, M.; Orane-Hutchinson, A. JUE Insight: The Determinants of the Differential Exposure to COVID-19 in New York City and Their Evolution over Time. *J. Urban Econ.* **2022**, *127*, 103293. [CrossRef]
108. Malik, O.; Gong, B.; Moussawi, A.; Korniss, G.; Szymanski, B.K. Modelling Epidemic Spread in Cities Using Public Transportation as a Proxy for Generalized Mobility Trends. *Sci. Rep.* **2022**, *12*, 6372. [CrossRef] [PubMed]
109. Hu, M.; Roberts, J.D.; Azevedo, G.P.; Milner, D. The Role of Built and Social Environmental Factors in COVID-19 Transmission: A Look at America's Capital City. *Sustain. Cities Soc.* **2021**, *65*, 102580. [CrossRef]
110. Jin, X.; Leng, Y.; Gong, E.; Xiong, S.; Yao, Y.; Vedanthan, R.; Wu, C.; Yan, L.L. Neighborhood-Level Public Facilities and COVID-19 Transmission: A Nationwide Geospatial Study in China. *medRxiv* **2020**.
111. Li, W.; Zhao, S.; Ji, X.; Ma, J. Impact of Traffic Exposure and Land Use Patterns on the Risk of COVID-19 Spread at the Community Level. *China J. Highw. Transp.* **2020**, *33*, 43–54. [CrossRef]
112. Wali, B.; Frank, L.D. Neighborhood-Level COVID-19 Hospitalizations and Mortality Relationships with Built Environment, Active and Sedentary Travel. *Health Place* **2021**, *71*, 102659. [CrossRef]
113. Johnson, T.F.; Hordley, L.A.; Greenwell, M.P.; Evans, L.C. Associations between COVID-19 Transmission Rates, Park Use, and Landscape Structure. *Sci. Total Environ.* **2021**, *789*, 148123. [CrossRef]
114. You, Y.; Pan, S. Urban Vegetation Slows down the Spread of Coronavirus Disease (COVID-19) in the United States. *Geophys. Res. Lett.* **2020**, *47*, e2020GL089286. [CrossRef]
115. Angel, S.; Lamson-Hall, P.; Salazar Tamayo, M.M. *Coronavirus and the Cities: Explaining Variations in the Onset of Infection and in the Number of Reported Cases and Deaths in US Metropolitan Areas as of 27 March 2020*; New York University, Marron Institute of Urban Management: New York, NY, USA, 2020.
116. Gatto, M.; Bertuzzo, E.; Mari, L.; Miccoli, S.; Carraro, L.; Casagrandi, R.; Rinaldo, A. Spread and Dynamics of the COVID-19 Epidemic in Italy: Effects of Emergency Containment Measures. *Proc. Natl. Acad. Sci. USA* **2020**, *117*, 10484–10491. [CrossRef] [PubMed]
117. Pierantoni, I.; Pierantozzi, M.; Sargolini, M. COVID 19—A Qualitative Review for the Reorganization of Human Living Environments. *Appl. Sci.* **2020**, *10*, 5576. [CrossRef]
118. Andersen, L.M.; Harden, S.R.; Sugg, M.M.; Runkle, J.D.; Lundquist, T.E. Analyzing the Spatial Determinants of Local COVID-19 Transmission in the United States. *Sci. Total Environ.* **2021**, *754*, 142396. [CrossRef] [PubMed]
119. Yu, D.; Li, X.; Yu, J.; Shi, X.; Liu, P.; Tian, P. Whether Urbanization Has Intensified the Spread of Infectious Diseases—Renewed Question by the COVID-19 Pandemic. *Front. Public Health* **2021**, *9*, 699710. [CrossRef] [PubMed]
120. Zhang, N.; Jia, W.; Wang, P.; Dung, C.-H.; Zhao, P.; Leung, K.; Su, B.; Cheng, R.; Li, Y. Changes in Local Travel Behaviour before and during the COVID-19 Pandemic in Hong Kong. *Cities* **2021**, *112*, 103139. [CrossRef]
121. Thaithatkul, P.; Sanghatawatana, P.; Anuchitchanchai, O.; Laosinwattana, W.; Liang, J.; Chalermpong, S. Travel Behavior Change of Public Transport Users during the COVID-19 Pandemic: Evidence from Bangkok. *Asian Transp. Stud.* **2023**, *9*, 100102. [CrossRef]
122. Aydin, N.; Kuşakcı, A.O.; Deveci, M. The Impacts of COVID-19 on Travel Behavior and Initial Perception of Public Transport Measures in Istanbul. *Decis. Anal. J.* **2022**, *2*, 100029. [CrossRef]
123. Oishi, S.; Cha, Y.; Schimmack, U. The Social Ecology of COVID-19 Cases and Deaths in New York City: The Role of Walkability, Wealth, and Race. *Soc. Psychol. Personal. Sci.* **2021**, *12*, 1457–1466. [CrossRef]
124. Wang, Y.; Tsai, T.C.; Duncan, D.; Ji, J. Association of City-Level Walkability, Accessibility to Biking and Public Transportation and Socio-Economic Features with COVID-19 Infection in Massachusetts, USA: An Ecological Study. *Geospat. Health* **2022**, *17*, s1. [CrossRef]
125. Wang, S.; Luo, X. The Evolution of Government Behaviors and Urban Expansion in Shanghai. *Land Use Policy* **2022**, *114*, 105973. [CrossRef]
126. Hamidi, S.; Ewing, R.; Sabouri, S. Longitudinal Analyses of the Relationship between Development Density and the COVID-19 Morbidity and Mortality Rates: Early Evidence from 1,165 Metropolitan Counties in the United States. *Health Place* **2020**, *64*, 102378. [CrossRef] [PubMed]
127. Ghosh, A.; Nundy, S.; Ghosh, S.; Mallick, T.K. Study of COVID-19 Pandemic in London (UK) from Urban Context. *Cities* **2020**, *106*, 102928. [CrossRef] [PubMed]
128. Mansour, S.; Al Kindi, A.; Al-Said, A.; Al-Said, A.; Atkinson, P. Sociodemographic Determinants of COVID-19 Incidence Rates in Oman: Geospatial Modelling Using Multiscale Geographically Weighted Regression (MGWR). *Sustain. Cities Soc.* **2021**, *65*, 102627. [CrossRef]
129. Gaskin, D.J.; Zare, H.; Delarmente, B.A. Geographic Disparities in COVID-19 Infections and Deaths: The Role of Transportation. *Transp. Policy* **2021**, *102*, 35–46. [CrossRef] [PubMed]
130. Tribby, C.P.; Hartmann, C. COVID-19 Cases and the Built Environment: Initial Evidence from New York City. *Prof. Geogr.* **2021**, *73*, 365–376. [CrossRef]
131. Kim, D. Exploratory Study on the Spatial Relationship between Emerging Infectious Diseases and Urban Characteristics: Cases from Korea. *Sustain. Cities Soc.* **2021**, *66*, 102672. [CrossRef]